Insight into the Reaction Mechanism and Deactivation during CO_2-Assisted Propane ODH over VO_x/TiO_2 Catalysts: An Operando Spectroscopic Study

Leon Schumacher, Kathrin Hofmann, Christian Hess*

Technical University of Darmstadt, Department of Chemistry, Eduard-Zintl-Institut für Anorganische und Physikalische Chemie, Peter-Grünberg-Str. 8, 64287 Darmstadt, Germany.

*Corresponding Author (E-Mail: christian.hess@tu-darmstadt.de)

Abstract

The CO_2-assisted oxidative dehydrogenation (ODH) of propane is of great interest for technical applications, enabling the use of the greenhouse gas CO_2 in a value-adding process. Supported vanadium oxide (VO_x) catalysts are a promising alternative to more active but toxic chromium oxide catalysts. Despite its common use, TiO_2 has not been investigated as support material for VO_x in the CO_2-assisted ODH of propane. In this study, we address the interaction between titania (P25) and vanadia within the reaction mechanism using XRD, multi-wavelength Raman, UV-Vis and DRIFT spectroscopy. Besides direct and indirect ODH reaction pathways, propane dry-reforming (PDR) is identified as a side reaction, which is more prominent on bare titania. The presence of VO_x enhances the stability and selectivity by participating in the redox cycle, activating CO_2 and leading to a higher rate of regeneration. As main deactivation mechanisms of the catalyst system we propose the reduction of the titania lattice and the consumption of vanadium, while carbon formation appears to be less relevant. Our results highlight the importance of analysing the CO_2-ODH reaction network and applying combined steady-state spectroscopies as a first step towards a detailed mechanistic understanding of CO_2-assisted propane ODH over supported VO_x catalysts.

1. Introduction

The oxidative dehydrogenation (ODH) of propane is a promising additional process towards propylene production to meet the ever growing demand for this base chemical.[1,2] This demand cannot be satisfied by traditional production methods like steam cracking or fluid catalytic cracking, resulting in the ‘propylene gap’.[3,4] The ODH of propane adds oxygen to the gas-feed, resulting in several advantages like lower reaction temperatures and therefore energy consumption and less catalyst leaching. However, it is still a challenge to control the oxidation process towards the selective oxidation product and significant amounts of CO_x are formed as a side product.[1,2,5] To avoid the over-oxidation of propane, CO_2 can be used as a soft-oxidant to increase the selectivity towards propylene. In addition, the heat capacity of CO_2 leads to a more homogenous temperature distribution throughout the reactor and a lower risk of flammability compared to O_2, facilitating a scale-up of the process.[6,7] From the environmental perspective, the use of the greenhouse gas CO_2 as a soft-oxidant in technical applications would directly assist in the efforts to mitigate the climate change, while creating value-added products in the form of propylene and CO.[8–10] However, due to the high temperature required for CO_2 activation,[11,12] a suitable catalyst needs to be employed to obtain sufficient conversions at moderate temperatures without catalyst deactivation (e.g. coking)[13].

A promising class of catalysts for the CO_2-assisted ODH of propane are supported transition metal oxide catalysts.[14–17] In the past, a research focus was put on chromium oxide (CrO_x) due to its high activity.[7,18–21] In this context, Mychorczyk et al.[20] described the oxidation state of chromium, as measured via operando UV-Vis spectroscopy, to be of great importance to differentiate between the oxidative and non-oxidative reaction paths, where Cr^{6+} species are reduced rapidly to $Cr^{2+/3+}$ species under reaction conditions, which participate in the non-oxidative pathway. However, as chromium oxides are toxic and harmful to the environment, other materials have attracted renewed interest.[22] Vanadium oxide (VO_x) is a promising catalyst for CO_2-assisted ODH reactions,[23–27] since it is commonly used for oxidation reactions in industrial applications and shows high activity for the ODH of propane using O_2.[5,28] Besides VO_x, molybdenum oxide (MoO_x) was recently used as the active phase.[29,30] For the vanadia-based catalysts, a variety of supports such as SiO_2,[23,27] Al_2O_3,[24] and In_2O_3[25,26] were already studied theoretically and experimentally in the literature. However, the use of CeO_2- and TiO_2-supported vanadia catalysts, which are the most active support materials in propane ODH using O_2,[31,32] has not been reported in the context of CO_2-assisted ODH reactions.

An important aspect towards mechanistic understanding is the characterization of the reaction network using CO_2-assisted propane ODH, as multiple side reactions, like propane dry reforming (PDR),[25] carbon formation, cracking, and coke gasing may occur simultaenously.[13] Furthermore, based on experimental and theoretical work on a WO_x-VO_x/SiO_2 catalyst, Ascoop et al.[23] proposed the occurrence of two pathways for propylene formation, that is a direct pathway via the ODH reaction and an indirect two-step pathway, including direct propane dehydrogenation, resulting in propylene and hydrogen, followed by a reaction of H_2 with CO_2 to CO and water via the reverse water-gas shift (RWGS) reaction. The presence of two simultaneous reaction pathways towards propylene was confirmed experimentally by Rogg et al.[27] for VO_x/SiO_2 catalysts, using operando spectroscopy, highlighting the importance of the pre-treatment conditions as partly reduced vanadia chains seem to limit the deep oxidation potential, increasing the propylene selectivity. Regarding the use of active support materials, Jiang et al.[25,26] have recently described the potential of VO_x/In_2O_3 catalysts, where vanadia was identified to reduce dry-reforming and participate in the redox cycle, resulting in good ODH selectivities. Monomeric VO_x species were proposed as the most active site, due to their strong interaction with indium.[26] However, despite these studies, there is a number of open questions related to the mode of operation of VO_x catalysts in CO_2-assisted propane ODH: What is the role of CO_2 within the reaction network? Is the support actively participating in the reaction? How can the selectivity behavior be explained and possibly controlled? How does the catalyst deactivate?

To answer these questions, we address the mode of operation of different VO_x/TiO_2 catalysts during CO_2-assisted propane ODH, by combining multiple quasi in-situ and operando methods in this study. These include multi-wavelength Raman, UV-Vis, and DRIFT spectroscopy, as well as XRD to gain insight into the reaction mechanism and to identify the exact role of CO_2 and the support, and to elucidate vanadia nuclearity-dependence of the observed reactivity behavior. The combination of these methods allows for a dedicated investigation of the active and support phases based on differing selective intensity enhancements and a differentiation between surface, subsurface, and bulk processes due to the different information depth of the applied methods. Furthermore, we address the common problem of catalyst deactivation during the reaction by identifying key catalyst deactivation mechanisms relevant to VO_x/TiO_2 catalysts. Our results demonstrate the great potential of combining multiple operando methods to provide a mechanistic understanding of catalytic reactions with potential industrial applicability. Our approach can readily be transferred to other catalyst materials based on ceria, molybdena or tungstia.

2. Experimental Section

2.1. Catalyst Preparation

Bulk titania and thin-film titania prepared by atomic layer deposition (ALD) was used as support material. Titania P25 (Aeroxide, Sigma-Aldrich, ≥99.5%), consisting of 77% anatase, 16% rutile, and 7% amorphous titania, was purchased.[33] The P25 samples were first characterized by nitrogen physisorption and subsequent analysis by the Brunauer-Emmet-Teller (BET) method, yielding a surface area of 73 m^2/g and then loaded by wet-impregnation using an aqueous solution containing a 1:2 ratio of ammonium meta vanadate (AMV) and oxalic acid with four different concentrations (1.2, 0.59, 0.25, and 0.05 mol/l), resulting in vanadium surface densities of 2.5, 1.2, 0.5, and 0.1 V/nm^2, respectively. All samples were loaded below monolayer loading (as confirmed by Raman analysis), thus guaranteeing that only amorphous vanadia was present.[34] The loaded samples were dried at 120 °C for 12 h and then calcined at 480 °C for 4 h.

Mesoporous silica SBA-15 was synthesized as described previously,[27] and coated with titania using a custom-built ALD set-up, as described previously.[28] The theoretical thickness of the thin-film titania corresponds to 10 nm, as determined by ellipsometry for a silicon wafer.[35] The sample was calcined in air at 600 °C for 12 h to crystallize the titania. The specific surface area was determined to be 81 m^2/g by nitrogen physisorption with subsequent BET analysis. The samples were also loaded by wet-impregnation, employing an aqueous solution with a 1:2 ratio of AMV and oxalic acid with a concentration of 0.67 mol/l, resulting in a vanadium surface density of 1.2 V/nm^2. The samples were dried and calcined as described above. All samples were prepared in the same exact way as in our previous VO_x/TiO_2 study on propane ODH using O_2, to guarantee comparability.[**28**]

2.2. Catalytic Testing

Catalytic testing was performed in a CCR 1000 reaction cell (Linkam Scientific) equipped with a membrane pump to allow for operation in a fluidized-bed mode, using 60 mg of catalyst for the P25 samples and, due to its much lower density, 25 mg of the ALD-synthesized samples. The samples were first dehydrated in 12.5% O_2/He for 1 h at 550 °C, subsequently cooled to 50 °C, exposed to 12.5% CO_2/12.5% C_3H_8/He with a total flow rate of 40 ml_n/min, and then heated in 45 °C steps up to 550 °C, staying at each temperature for 1 h. The gas-phase composition was analyzed continuously using a gas chromatograph (GC, Agilent Technologies 7890B) equipped with a PoraPlotQ and a Molsieve column as well as a thermal conductivity detector (TCD) and a flame ionization detector (FID) in series. The set-up is connected through a twelve-way valve. One chromatogram is measured every 29 min, resulting in two chromatograms for each temperature, which were averaged. The pressure before and after the GC was monitored to correct the detected areas for pressure fluctuations. The obtained conversions were normalized to the surface area of the catalyst, due to the significantly different sample masses used for P25 and ALD-synthesized catalysts. To analyze the reaction network, the temporal evolution of the reactivity behavior was analyzed at 550 °C. The samples were first dehydrated in 12.5% O_2/He for 1 h, then treated consecutively in 7.5% H_2/Ar, 12.5% CO_2/He, 12.5% CO_2/12.5% C_3H_8/He, and finally regenerated in 12.5% CO_2/He (for 2 h for each gas phase), respectively. The reaction products were analyzed and time-dependent ratios between different products were calculated to determine the relative contributions of the different reaction pathways to the overall product distribution.

2.3. UV-Raman Spectroscopy

UV-Raman spectroscopy was performed at an excitation wavelength of 385 nm generated by a laser system based on a Ti:Sa solid-state laser pumped by a frequency-doubled Nd:YAG laser (Coherent, Indigo). The fundamental wavelength is frequency doubled to 385 nm using a LiB_3O_5 crystal. The light is focused onto the sample, and the scattered light is collected by a confocal mirror setup and focused into a triple-stage spectrometer (Princeton Instruments, TriVista 555).[36] Finally, the Raman contribution is detected by a charge-coupled device (CCD, 2048 × 512 pixels) cooled to –120 °C. The spectral resolution of the spectrometer is 1 cm^{-1}. For Raman experiments, 60 mg of catalyst was placed in a CCR 1000 reactor (Linkam Scientific Instruments) equipped with a CaF_2 window (Korth Kristalle GmbH). A fluidized-bed reactor was employed to avoid laser-induced damage, allowing the use of a laser power of 8 mW at the location of the sample. Data processing included cosmic ray removal and background subtraction. Operando spectra were measured after dehydration for 1 h in 12.5% O_2/He and further pre-treatment in 7.5% H_2/Ar and 12.5% CO_2/He at 550 °C to start from a partially oxidized state. Afterwards, the catalyst was exposed to reactive conditions (12.5% CO_2/12.5% C_3H_8/He) and regenerated under oxidizing conditions (12.5% CO_2/He) with a total flow rate of 40 ml_n/min for each gas phase. The spectra were further analyzed by a least-squares fitting analysis using Lorentzian functions after normalization to the anatase E_g peak at 630 cm^{-1}. The intensity of the carbon signal was determined by integration over all carbon peaks.

2.4. Vis-Raman Spectroscopy

Visible (Vis) Raman spectroscopy was performed at 514 nm excitation, emitted from an argon ion gas laser (Melles Griot). The light was focused onto the sample, gathered by an optical fiber, and dispersed by a transmission spectrometer (Kaiser Optical, HL5R). The dispersed Raman radiation was subsequently detected by an electronically cooled CCD detector (–40 °C, 1024 × 256 pixels). The spectral resolution was 5 cm^{-1} with a wavelength stability of better than 0.5 cm^{-1}. For Raman experiments, 60 mg of catalyst was filled into a CCR 1000 reactor (Linkam Scientific Instruments) equipped with a quartz window (Linkam Scientific Instruments). A fluidized-bed reactor was employed to avoid laser-induced damage, allowing the use of a laser power of 5 mW at the location of the sample. Data analysis of the Raman spectra included cosmic ray removal and an auto new dark correction. Operando spectra were measured after dehydration in 12.5% O_2/He and further pre-treatment in 7.5% H_2/Ar and 12.5% CO_2/He at 550 °C for 1 h, respectively, to start from a partially oxidized state. Afterwards, the catalyst was exposed to reactive conditions (12.5% CO_2/12.5% C_3H_8/He) for 2 h for time-dependent measurements and regenerated under oxidizing conditions (12.5% CO_2/He) for 1 h with a total flow rate of 40 ml_n/min for each gas phase. The spectra were further analyzed by a least-squares fitting analysis using Lorentzian functions after normalization to the anatase E_g peak at 630 cm^{-1}.

2.5. X-Ray Diffraction

Powder X-ray diffraction (XRD) patterns were recorded on a Stadi-P (Stoe & Cie) diffractometer with a Ge(111)-monochromator, Cu $K\alpha_1$ radiation (λ = 1.54060 Å), and a MYTHEN-1K (Dectris) detector, using a flat sample holder in transmission geometry. For quasi in-situ XRD measurements the samples were measured in pristine condition after dehydration in 12.5% O_2/He for 1 h at 550 °C, followed by rapid cooling to room temperature in pure helium in the Linkam reactor and an inert transfer to the diffractometer. For the second set of experiments, the samples were pre-treated consecutively in 12.5% O_2/He, 7.5% H_2/Ar, 12.5% CO_2/He, and 12.5% CO_2/12.5% C_3H_8/He for 1 h at 550 °C, respectively, followed by rapid cooling to room temperature (200 °C/min) in pure helium in the Linkam reactor and an inert transfer to the diffractometer.

2.6. Diffuse Reflection UV-Vis Spectroscopy

Diffuse reflectance (DR) UV-Vis spectra were recorded on a Jasco V-770 UV-Vis spectrometer. Dehydrated $BaSO_4$ was used as the white standard and 75 mg of catalyst were placed in the commercially available reaction cell (Praying Mantis High Temperature Reaction Chamber, Harrick Scientific) equipped with transparent quartz glass windows for each experiment. Operando spectra were measured after dehydration in 12.5% O_2/He and further pre-treatment in 7.5% H_2/Ar and 12.5% CO_2/He at 550 °C for 1 h, respectively, to start from a partially oxidized state. Afterwards, the catalyst was exposed to reactive conditions (12.5% CO_2/12.5% C_3H_8/He) for 1.5 h for time-dependent measurements and regenerated under oxidizing conditions (12.5% CO_2/He) at 550 °C for 1 h with a total flow rate of 40 ml_n/min for each gas phase. The spectra were further analyzed by a least-squares fitting analysis using Gaussian-Lorentzian (70/30) product functions. Product functions were used to account for the large contribution of natural line broadening to the overall line-shape, caused by the short life-time of the electronically excited states (Lorentzian), while also accounting for the generally better convergence of the fit (Gaussian).[37] The band gap energies were determined using Tauc plots.[38,39]

2.7. Diffuse Reflection Infrared Fourier Transform Spectroscopy

Diffuse reflectance infrared Fourier transform spectroscopy (DRIFTS) was performed using a Vertex 70 spectrometer (Bruker). A liquid nitrogen-cooled mercury cadmium telluride (MCT) detector was used, operating at a resolution of 1 cm^{-1}. Dehydrated potassium bromide was employed as an infrared transparent sample for the background spectrum. For each experiment, 75 mg of catalyst was placed in the commercially available reaction cell (Praying Mantis High Temperature Reaction Chamber, Harrick Scientific) equipped with transparent KBr windows.

For quasi in-situ measurements the samples were treated in 12.5% O_2/He, 7.5% H_2/Ar, 12.5% CO_2/He, 12.5% CO_2/12.5% C_3H_8/He, and finally regenerated in 12.5% CO_2/He for 1 h at 550 °C, respectively. For each gas phase the sample was cooled rapidly to room temperature (200 °C/min) in pure helium in the Linkam reactor for the measurement before heating it back to 550 °C for the next measurement.

Data processing consisted of background removal by subtracting a baseline formed by 12 anchor points and removal of the spectrum recorded in 12.5% O_2/He to subtract the contributions from the pristine catalyst, targeting the surface species formed by the additional gas treatments only. Finally, to quantify the adsorbate peaks in the vanadyl and Ti-OH regions, the spectra were fitted using Lorentzian functions employing the Levenberg-Marquardt algorithm implemented in OriginLab 2022b.

3. Results and Discussion

Reactivity Behavior and Analysis of the Reaction Network

To choose a temperature that is most ideal for the operando spectroscopic investigation of the CO_2-assisted ODH of propane over VO_x/TiO_2, a temperature-dependent analysis of the catalytic activity was performed. Figure 1 summarizes the catalytic performance between 45 and 550 °C, showing the propane conversions (left panel) and selectivities to propylene (right panel).

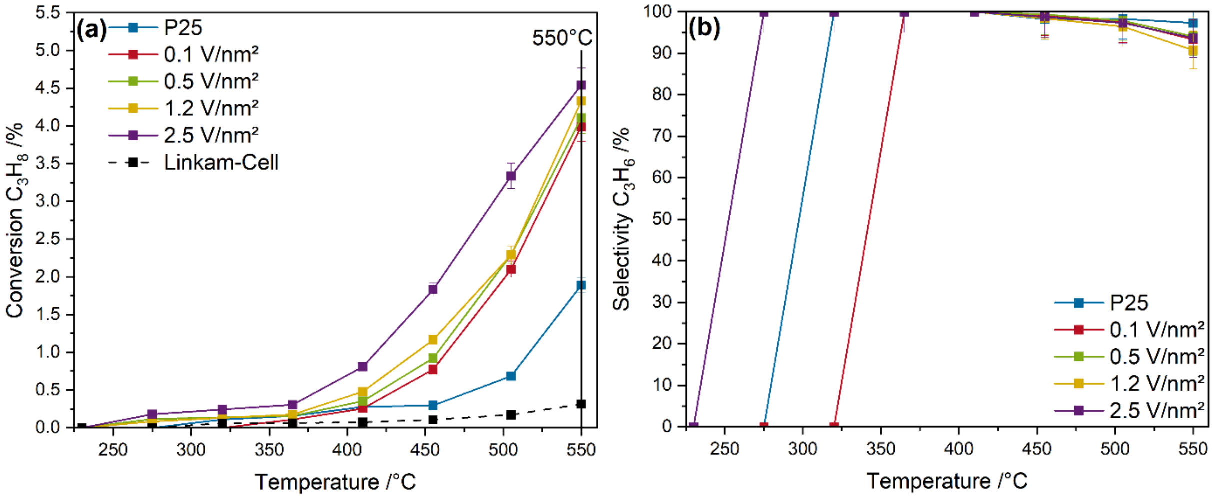

Figure 1: Reactivity behaviour of VO_x/TiO_2 catalysts in CO_2-assisted propane ODH. Temperature-dependent **(a)** conversion of propane and **(b)** selectivity towards propylene of the bare TiO_2 P25 support, the vanadia-loaded samples, and the empty Linkam reactor recorded in a feed of 12.5% CO_2/12.5% C_3H_8/He (total flow rate: 40 ml/min). The black line (left panel) highlights the temperature chosen for the mechanistic analysis.

Figure 1a depicts the temperature-dependent conversion of propane, starting at 275 °C for the three samples with the highest vanadium loading and at 320 °C for the P25 and P25+0.1 V/nm² samples. The conversion then increases exponentially with the increasing temperature up to 550 °C, where the catalysts reach propane conversions between 2.35 % (bare P25) and 4.54 % (P25+2.5 V/nm²), showing an increase with increasing vanadium loading. Importantly, the onset of propane conversion jumps from P25 to P25+0.1 V/nm², indicating that the presence of vanadium greatly increases the catalytic activity. The propane conversion of the empty Linkam reactor (0.31 %) is small compared to that of the VO_x/TiO_2 catalysts. The homogeneous gas-phase reaction occurring in the reactor does not lead to the formation of propane, but rather mostly

C_2H_4, CH_4, and CO, indicative of mostly cracking or total oxidation reactions. Therefore, the ODH reaction is determined to be exclusively caused by the catalysts. In general, the P25+2.5 V/nm² sample is the most active, showing the earliest onset of the reaction, and a significantly higher propane conversion than the other samples, while the other three VO_x/TiO_2 samples, show a somewhat similar conversion behaviour. The conversions are in the same order of magnitude compared those obtained under similar conditions (vanadia loading, catalyst mass, temperature) in a fixed bed reactor.[25] However, due to a lack of literature data, a direct comparison to other titania catalysts is not possible. The selectivities remain at 100 % for temperatures up to 410 °C, while at higher temperatures, the selectivity drops to an absolute minimum of 91% for the P25+1.2 V/nm² sample at 550 °C, which compares very favourably with other vanadia-based catalysts.[23–25,27] Therefore, a reaction temperature of 550 °C was chosen for the mechanistic analysis.

To analyse the reaction network in more detail, the catalytic activity of the samples was determined at 550 °C in 12.5% CO_2/12.5% C_3H_8/He, after dehydration at 550 °C in 12.5% O_2/He for 1 h and pre-treatment in 7.5% H_2/Ar and 12.5% CO_2/He, to establish a partially reduced initial state, that is more representative of the state at which the catalyst will be operating during the reaction. Afterwards, the samples are regenerated in 12.5% CO_2/He. The molar product distributions for all gas phases of the P25-based samples are given in the SI (see Figure S1). The most important kinetic results used to differentiate the different reactions occurring on the catalyst are given in Figure 2.

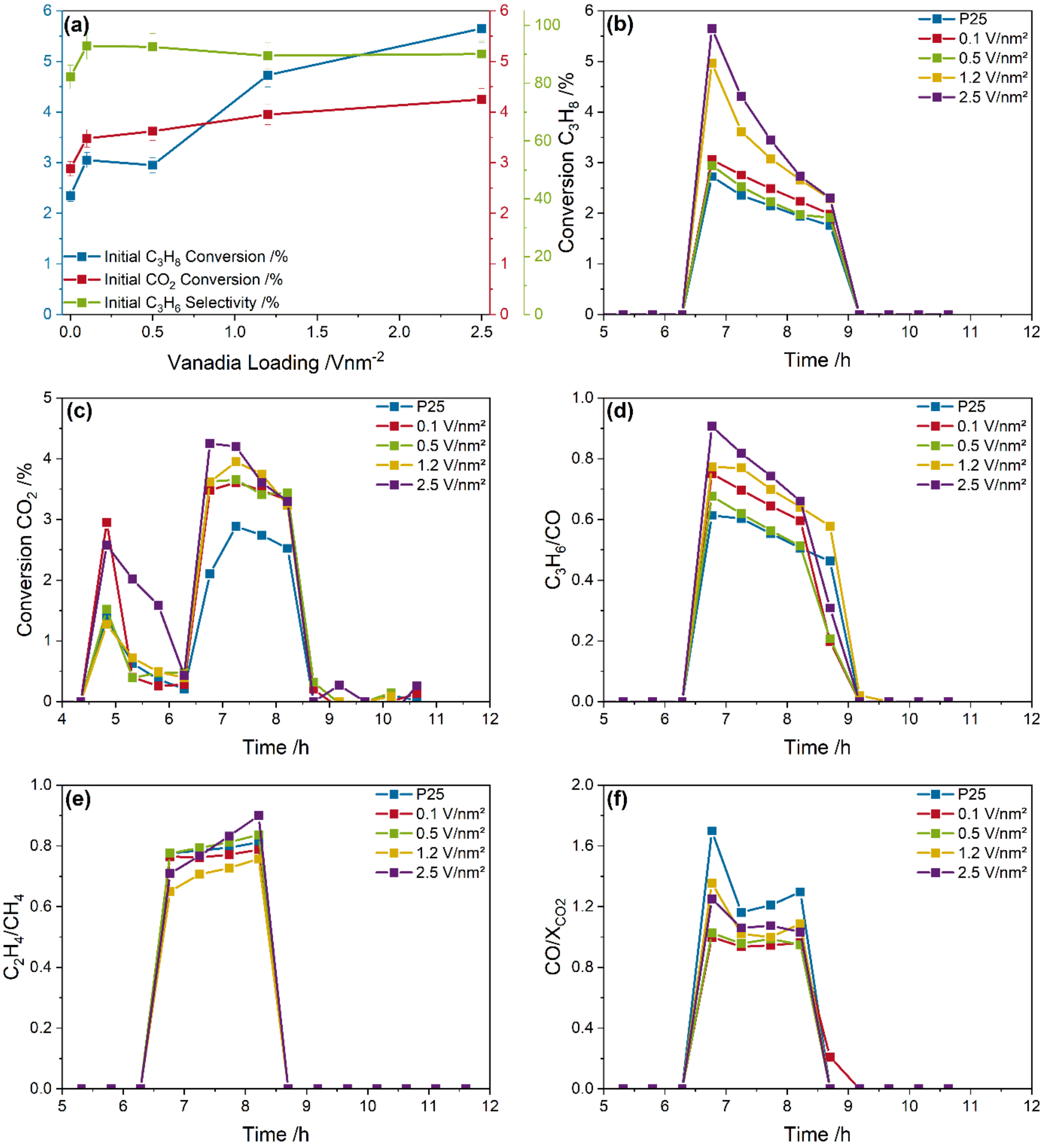

Figure 2: Analysis of the reaction network for bare P25 and vanadia-loaded samples during CO_2-assisted propane ODH: **(a)** Loading-dependent initial conversions of C_3H_8 and CO_2, and C_3H_6 selectivity, **(b)**+**(c)** time-dependent conversions of C_3H_8 and CO_2, **(d)** time-dependent C_3H_6/CO ratio, **(e)** time-dependent C_2H_4/H_2 ratio, and **(f)** time-dependent CO/X_{CO2} ratio. Between 0 and 2 h 12.5% O_2/He, between 2 and 4 h 7.5% H_2/Ar, between 4 and 6 h 12.5% CO_2/He, between 6 and 9 h 12.5% CO_2/12.5% C_3H_8/He, and between 9 and 11 h 12.5% CO_2/He were used as the gas feed.

Figure 2a depicts the loading-dependent initial conversions of C_3H_8 and CO_2, as well as the initial C_3H_6 selectivity for the bare P25 support and the VO_x/TiO_2 samples, obtained at 550 °C after pre-treatment in O_2, H_2, and CO_2 for 1 h each (see experimental section for details). Starting at 2.35% for P25, the C_3H_8 conversion increases with the vanadium loading up to 5.65% for P25+2.5 V/nm², after showing a distinct jump from P25 to P25+0.1 V/nm² and from 0.5 to 1.2 V/nm². In contrast, the CO_2 conversion starts at 2.88% for P25 and then increases to a maximum of 4.25% for P25+2.5 V/nm², staying slightly above the C_3H_8 conversions at all vanadium loadings, except for the P25+2.5 V/nm² sample, indicative of side reactions, such as PDR or cracking, as the dehydrogenation pathways would consume propane and CO_2 at the same rate. In comparison to the propane conversion, the CO_2 conversion increases almost linear with the vanadium loading and exhibits no plateau between 0.1 and 0.5 V/nm². Similar to the conversions, the initial selectivities towards propylene jump from bare P25 to the P25+0.1 V/nm² sample increasing from 82.2% for P25 to 92.9%. It then decreases again to 90% for the P25+2.5 V/nm² sample. These selectivities already include the PDR side reaction, which is discussed below. However, the selectivities are high at >80% and do not fluctuate significantly. Therefore, the presence of vanadium seems to mostly increase the rate of propylene formation. Overall, the initial values of propane and CO_2 conversions in combination with the propylene selectivities are at a higher level than those of other VO_x-based catalyst systems,[23–25,27] and even reach those of some of the supported CrO_x systems.[18,21,40]

Figures 2b and c depict the time-dependent conversions of C_3H_8 and CO_2 for the P25-based samples. As shown in Figure 2b, the propane conversion is significantly higher at the beginning of the reaction, which is most pronounced for the samples loaded with 1.2 and 2.5 V/nm². The C_3H_8 conversion decreases to a similar value of around 2% for all samples after ~3h (P25: 1.75%, P25+2.5 V/nm²: 2.4%), but still follows the same trend of a conversion, which increases with the vanadium loading. Thus, the decrease in propane conversion is most significant for the samples with the highest loadings. In comparison, the CO_2 conversion stays more constant during the reaction, except for the P25+2.5 V/nm² sample. This is a first indicator that catalyst reoxidation with CO_2 is rate-limiting, that is, the catalyst decreases its overall activity due to an overall catalyst reduction. After the initial 30 minutes, the CO_2 conversion is similar to that of propane for all samples, except for the P25 sample, indicating the occurrence of more side reactions on the bare support. However, since the propane conversion gradually decreases further and the CO_2 conversion stays more constant, the CO_2 conversion is, at the end of the reaction phase, higher than that of propane. This indicates a deactivation of the catalyst for the ODH reaction, with reoxidation being the rate-limiting step.

For further analysis of the reaction network, the relative amount of different reactions occurring on the catalyst surface and the importance of the ODH route was studied. To this end, Figures 2d-f show the C_3H_6/CO ratio, as an indicator for the extent of dehydrogenation, the C_2H_4/CH_4 ratio, as an indicator for the amount of cracking, and the CO/X_{CO2} ratio, as an indicator for PDR, respectively. The time-dependent molar product distributions are given in Figure S1. Starting with the C_3H_6/CO ratio, the values decrease over time due to the decreasing propane conversion. The initial values are lowest for bare P25 (0.61) and highest for P25+2.5 V/nm^2 (0.91), following an increase with increasing vanadium loading. At the end of the reaction phase, values drop to 0.46 for P25 and 0.66 for P25+2.5 V/nm^2. Generally, more CO than propylene is produced. Since the C_3H_6 to CO ratio should be 1 for the direct (ODH) and indirect (DDH+RWGS) reaction routes, additional reactions are expected to occur. This is supported by the observed CO_2 conversions, which are consistently higher than those of propane. However, the ratio is, especially for the P25+2.5 V/nm^2 sample, close to a value of one, indicating a full dehydrogenation route over the catalyst, in good agreement with other actively supported VO_x systems,[24–26] which show side reactions in a similar range, but the TiO_2 system seems to be slightly more selective towards propylene.

To gain insight into the side reactions, Figure 2e depicts the C_2H_4 to CH_4 ratio, which is indicative of propane cracking, leading to ethylene and methane. The ratio is close to one with slightly more methane being produced, which is in agreement with the expected product distribution of thermal propane cracking at this temperature.[41] It is important to note that the overall amount of ethylene and methane is comparably small, especially when considering the fact that one methane and one ethylene molecule are produced from one propane molecule. In fact, the amount of cracking is determined to be <5% of the overall conversion for all samples, based on the molar product distributions (see Figure S1). Furthermore, around ~50% of the detected methane and ethylene (depending on the sample) is produced by the empty reactor, further decreasing the relevance of propane cracking on the catalyst. While the C_2H_4 to CH_4 ratio increases with propane conversion, the overall extent of cracking slightly decreases, which is in good agreement with the ~2% cracking occurring on the catalyst itself, while half of these products are formed by the reactor, which should have a constant product distribution. The slight increase in the $C2H_4$ to CH_4 ratio towards the end of the reaction phase is in good agreement with the less conversion via the ODH reaction, which is exothermic in nature.[42] As a result, the amount of reaction heat is decreased and the temperature of the system is also slightly decreased (a few degrees), which shifts the cracking products towards ethylene.[41] Overall, due to its weak contribution, propane cracking is considered as less important for the overall reaction network and the behavior of the catalyst.

Last, Figure 2f shows the ratio between the produced CO and the converted CO_2 (CO_2 based CO selectivity), as an indicator for PDR. For bare P25, within the first 30 minutes, 70% more CO is produced than CO_2 is converted, indicating a high degree of PDR, which then decreases to a stable level of around ~25% more CO. While the ODH/DDH+RWGS should create one CO molecule each, this always converts a CO_2 molecule. Therefore, the excess CO must be produced from propane by PDR. This behaviour might be indicative of highly reducible active sites for the PDR reaction that are quickly consumed, leading to a stable level of CO production. In comparison, the vanadia-loaded samples depict a CO_2 based CO selectivity that is only slightly above one (1.02-110), indicating a small contribution of PDR but to a much smaller degree as for bare P25. A similar behaviour was previously observed for supported vanadia systems and explained by the acid-base properties of the system, as the introduction of vanadia as an acidic oxide increases the rate of C-H bond activation in comparison to the more basic support, in this case TiO_2, which activates the C=O bond.[25] In principle, such a scenario is consistent with the results observed here for the VO_x/TiO_2 system. Considering the loading dependence the reactivity behaviour of the 0.1 and 0.5 V/nm² samples is characterized mainly by the ODH of propane, whereas the 1.2 and 2.5 V/nm² samples show slightly higher ratios (~1.1) and also exhibit a much higher ratio in the first 30 minutes, indicating structural and/or chemical changes on the surface, which influences the PDR rate. The loading-dependent behaviour may be caused by the different vanadia nuclearity distributions, which has been shown to vary significantly for VO_x/TiO_2 catalysts.[28] For example, oligomers, present on the P25+2.5 V/nm² sample, are more reducible and prone to less selective oxidation as compared to monomers and dimers.[28]

During the reaction, a significant amount of hydrogen is formed (see Figure S1), which increases with the vanadium loading. To explain this behaviour, the following two scenarios are conceivable: First, hydrogen formed by the direct dehydrogenation of propane, might not be fully converted to H_2O in the RWGS, as titania is typically a good RWGS reaction catalyst only in combination with a metal.[43,44] The second scenario is based on the formation of carbon during the dry reforming process, resulting in a conversion of propane to CO, methane, hydrogen, and carbon coking on the catalyst surface.[45] The plethora of different PDR reaction products can explain the presence of free hydrogen and might also explain the higher amount of methane than ethylene produced during cracking. In addition, the main product, CO, explains the higher amount of detected CO than converted CO_2 (see Figure 2f). The presence of carbon on the catalyst during the reaction will be discussed in more detail in the operando spectroscopy section. Due to the different possibilities for the hydrogens origin, the H_2/CO ratio to determine the amount of DDH vs ODH is not feasible in this context.

Additionally, to compare the results of a bulk TiO_2 to a different TiO_2-based support material, we exposed vanadia-loaded TiO_2/SBA-15 (SBA15-T) samples prepared by ALD to the same gas-treatments to investigate their catalytic behaviour. The results are given in the SI (see Figures S2 and S3). While the samples show less conversion than the corresponding P25-based samples discussed above, the difference between the vanadia-loaded sample and the bare support regarding C_3H_8 conversion is much less pronounced than for the P25-based samples. An important feature of the ALD-based TiO_2 material is that its propane conversion stays much more stable than that of bulk TiO_2, which shows a rapid decrease with time on stream. The propane and CO_2 conversions are very similar for both materials, while significantly more CO than propylene is produced, which is supported by the CO_2-based CO selectivity, which reaches a maximum of 285% for the SBA15-T+1.2 V/nm^2 sample, indicating a strong contribution of PDR. Bare SBA15-T, on the other hand, rather follows selective dehydrogenation pathways and is more directly comparable to the bulk TiO_2, while maintaining a stable C_3H_8 and CO_2 conversion.

In summary, the VO_x/TiO_2 systems show a good catalytic activity, with overall selectivities above 90% for the vanadia-loaded samples. Typical side reactions like PDR are of relevance on the bare support where significantly more CO is produced than CO_2 is converted, indicating that some propane is consumed to form CO. When vanadia is introduced, the PDR rates are reduced significantly, allowing for an almost exclusive dehydrogenation of propane via either ODH or DDH+RWGS reaction pathways. The presence of free H_2 indicates the occurrence of some PDR that also produces CH_4 and carbon on the catalyst surface, which will be subject to operando spectroscopic analysis (see below).

Operando Spectroscopy

To gain insight into the reaction mechanism, multiple operando spectroscopies were employed during the different gas feeds (compare experimental section). However, since the propane conversion, especially on the vanadia-loaded samples, does not stay constant and the measurements of different operando/quasi in situ methods occur on different time scales, each method may probe a different state of the catalyst. Therefore, multiple spectra of methods with short acquisition times (Vis-Raman: 30 min, UV-Vis: 5 min) were recorded, to obtain time-dependent insight into the catalyst behaviour, while methods requiring longer acquisition times (UV-Raman: 120 min) were applied in a more integral manner. To further clarify this point Figure S4 gives an temporal overview of the time of measurement of operando UV-Raman, Vis-Raman, and UV-Vis spectra in comparison to the molar product distributions for P25 and P25+1.2 V/nm^2.

Starting with UV-Raman spectroscopy, Figure 3 shows spectra of bare P25 and P25+1.2 V/nm^2 recorded at 385 nm excitation, as well as the results of a quantitative analysis of the observed spectral changes. The UV-Raman spectra for the other vanadia-loaded P25 samples and the ALD-based samples are given in the SI (see Figures S5 and S6).

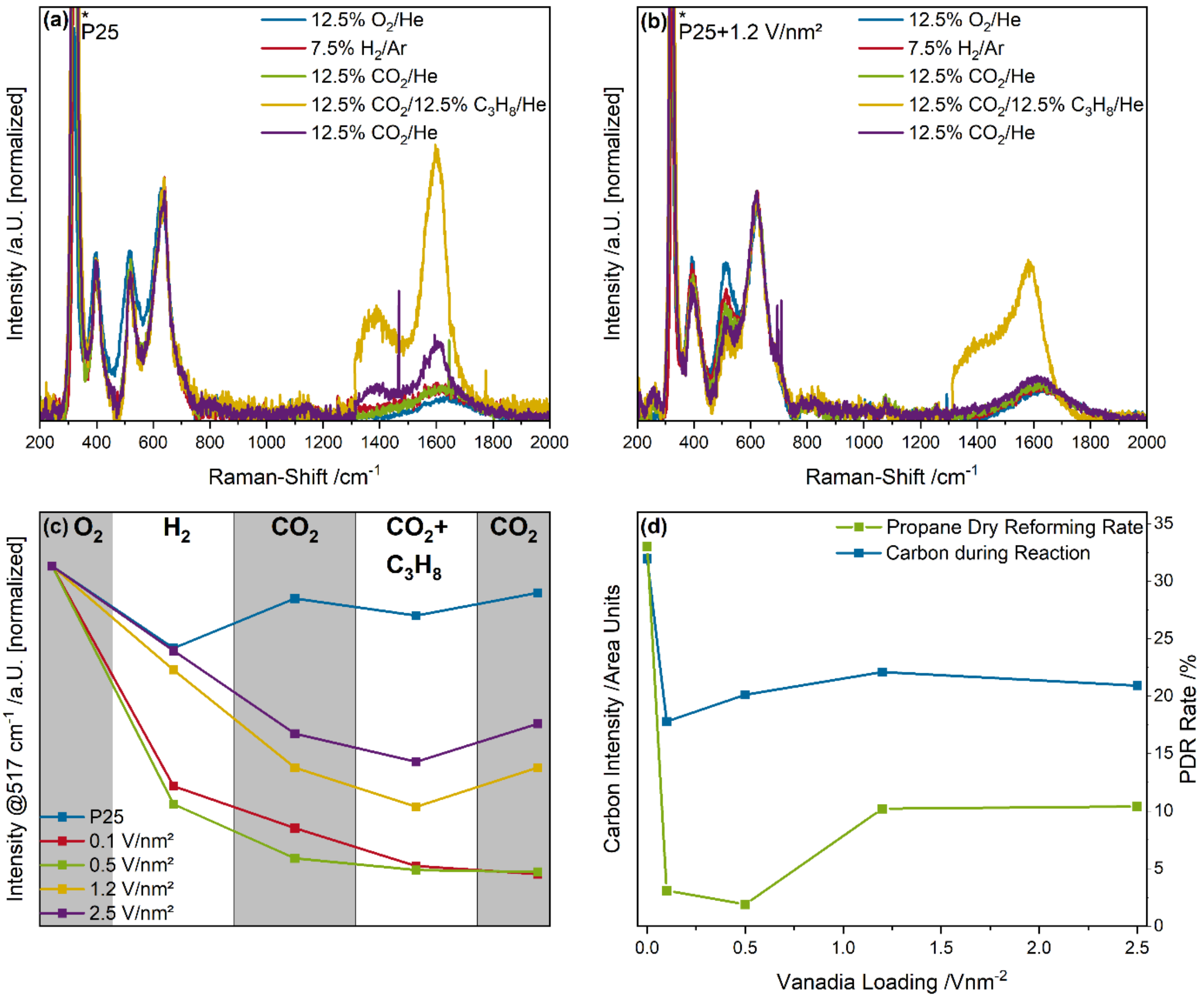

Figure 3: Operando UV-Raman spectra at 385 nm excitation of **(a)** P25 and **(b)** 1.2 V/nm² recorded at 550 °C in different gas feeds (see experimental section). Spectra were normalized to the E_g phonon of anatase at 630 cm^{-1}. The signal marked with an asterisk is caused by the CaF_2 spectroscopic window. The anatase phonon intensity **(c)** and the amount of amorphous carbon detected during reaction conditions **(d)** were quantified and compared to the PDR rate.

Figure 3a shows the UV-Raman spectra of bare P25 at 550 °C for different gas feeds. During the three pre-treatment gas feeds, that is O_2/He, H_2/Ar, and CO_2/He, the most significant spectral changes are detected for the B_{1g} and A_{1g} phonons of anatase at 398 and 517 cm^{-1}, respectively,[46] which decrease in intensity in the hydrogen phase and stay constant afterwards. When propane is introduced, a significant amount of carbon appears on the catalyst surface, which cannot be fully removed in the 2 h regenerative CO_2 treatment after the reaction, indicating a slow oxidation of carbon by CO_2. The P25+1.2 V/nm² sample shows a more pronounced decrease in its anatase phonon intensity, especially the A_{1g} phonon. Additionally, the formation of carbon is observed during reaction conditions, which however is fully regenerated by the CO_2

phase after reaction. The overall amount of deposited carbon during the reaction is smaller than for bare titania, indicating a higher rate of oxidation, which correlates with the increased conversion. The P25 samples loaded with 0.1, 0.5, and 2.5 V/nm² (see Figure S5) show similar structural dynamics to different extents, which is quantified in Figures 3c and d. Notably, no vanadia signals are observed in the UV-Raman spectra, indicating that the high temperature and absorbance of titania inhibits their detection.

The phonon band at 517 cm^{-1} was used as an indicator for the surface reduction of the samples. Its selective decrease at 517 cm^{-1} was observed previously observed and is caused by two factors.[47,48] The first factor is the integration of vanadia into the titania lattice as detected during the phase transition from anatase to rutile introducing a doped metal atome that distorts the lattice of titania.[49] The second is, the unilateral disturbance in the local order of the lattice, resulting from a reduction of the lattice with an oxygen gradient towards the surface.[48] However, no phonons of rutile were observed since their intensity is smaller than those of anatase and the temperature at which the experiments were performed leads to a lower signal to noise ratio.[46] Furthermore, due to the different absorption behavior, anatase absorbs stronger in the UV region, which leads to different resonance enhancements for anatase and rutile. Due to the strong absorption of titania at 385 nm, a quantification of the anatase phase is only possible at the catalyst surface, while the subsurface and bulk will be discussed later.[50–52] The phonon intensity of all samples decreases significantly upon reduction of the material via reaction of lattice oxygen with hydrogen to water, which is released from the catalyst surface into the gas phase. The surface of bare P25 is least reduced, while the samples with loading densities of 0.1 and 0.5 V/nm² become much more reduced, leading to an almost complete disappearance of the anatase phonon at 517 cm^{-1}. With increasing vanadium loading, the degree of reduction decreases again. This indicates that vanadia increases the surface reduction at low loadings while increasing the conversion, whereas at higher loadings the reduction might shift from the titania to the vanadia species present at that loading, thus reducing the titania surface to a smaller extent.

Figure 3d shows the integrated carbon signal during reaction as a function of vanadium loading and its comparison with the observed PDR rate (percentage of CO formed from C_3H_8), indicating that the carbon formation is not necessarily a function of the oxygen mobility in the sample but rather of the PDR activity, which is high in P25, decreases at low vanadia loadings, and increases again at higher loadings. However, a combination of both mechanisms seems most likely, as the samples loaded with 0.1 and 0.5 V/nm² show no PDR and still form a significant amount of carbon on the surface. Therefore, the reduction of the catalyst might lead to an increased amount of carbon in addition to a high level of PDR. The vanadia-loaded samples show less carbon deposition, which can only be explained by a higher rate of surface reduction, while the subsurface/bulk might be less reduced due to increased surface regeneratio using CO_2, facilitated by vanadia.

Notably, for the P25+2.5 V/nm² sample (see Figure S5), the V-O-V and V=O peaks are visible during the initial oxidative phase, but disappear for the other gas feeds, only regenerating slightly at 920 cm^{-1} for the regenerative CO_2 phase, indicating V-O-V participation.[53] The peak at 860 cm^{-1}, representing the V-O-Ti signal is also present (as for the P25+1.2 V/nm² sample), but does not change upon switching between the different gas feeds.[54] Therefore, the results indicate that similar vanadia species as during the propane ODH using O_2 are participating in the reaction.[28] A detailed analysis of the vanadyl region will be performed on the basis of DRIFTS data (see below).

The UV-Raman spectra of the ALD-based samples (see Figure S6) also shows carbon formation on the surface but no structural changes of the titania phonons. The vanadyl peak is clearly visible for the SBA15-T+1.2 V/nm² sample during initial oxidative conditions, as well as under CO_2 exposure, indicating vanadyl reduction and reoxidation.

To further understand the reduction of titania, the anatase E_g shift was determined from Vis-Raman spectra (see Figures S7 and S8) as an indicator of titania subsurface reduction.[55,56] The results are shown in Figure 4. The Vis-Raman spectra of the ALD-based samples are given in Figure S9.

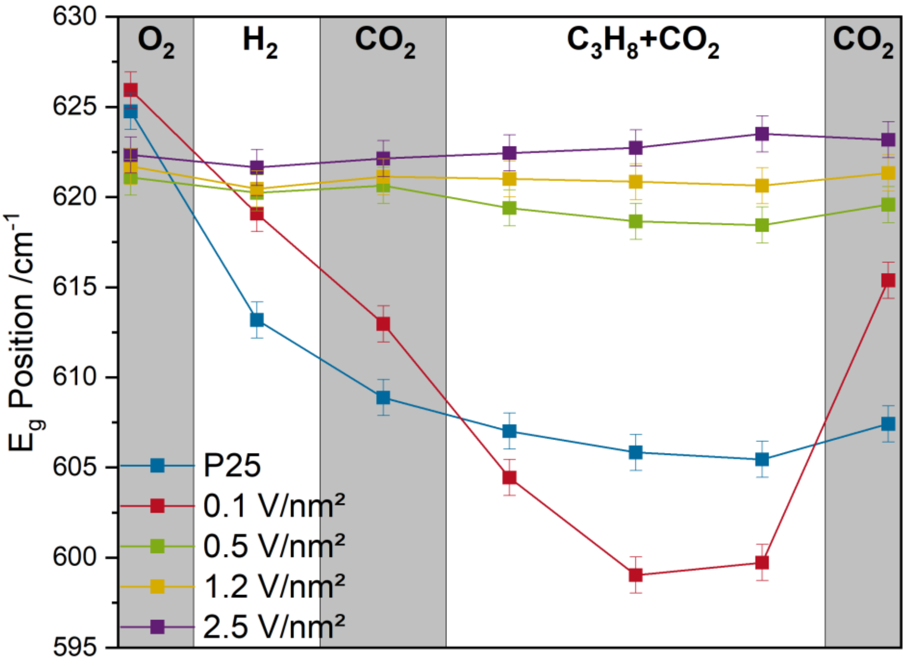

Figure 4: Position of the anatase E_g phonon determined from operando Vis-Raman spectra (at 514 nm excitation) recorded during exposure to 12.5% O_2/He, 7.5% H_2/Ar, 12.5% CO_2/He, 12.5% CO_2/12.5% C_3H_8, and 12.5% CO_2/He. The spectra are given in the SI (see Figures S7 and S8).

The E_g position of bare P25 strongly red-shifts when switching from the 12.5% O_2/He to the 7.5% H_2/Ar feeds, only red-shifting slightly further in the following CO_2-containing feeds, while it blue-shifts again in the last regenerative 12.5% CO_2/He phase. In comparison, the P25+0.1 V/nm² sample red-shifts less in its intensity in the first three pre-treatment phases, but red-shifts even stronger under reaction conditions, indicating strong sub-surface reduction of titania. It is then regenerated more significantly than for bare P25 in the last CO_2/He phase, indicating a stronger activation of CO_2 on the vanadia-loaded catalyst, which is likely caused by the short vanadia species present on the sample.[28] At vanadia loadings higher than 0.1 V/nm², no shift of the E_g position is observed. In agreement with the UV-Raman results, the P25 and 0.1 V/nm² sample show a similar behavior, pointing to a reduction of the surface and subsurface, while the P25+0.5 V/nm² sample shows the strongest surface reduction, but exhibits no subsurface reduction. For the 1.2 and 2.5 V/nm² samples no subsurface reduction is detected, while the surface reduction is less pronounced than that for the 0.5 V/nm² sample. This indicates that part of the redox cycle shifts from titania to surface-located vanadia and/or that CO_2 is much more easily activated over the

VO_x/TiO_2 samples, which increases the rate of regeneration of titania by gas phase CO_2, necessitating less oxygen diffusion within the support.

To obtain a more integral picture of the titania reduction, as well as potential phase-transformation of titania to the rutile phase, which is difficult to observe in the Raman spectra, quasi in situ XRD of P25 and the 1.2 V/nm² sample were recorded (see Figure 5).

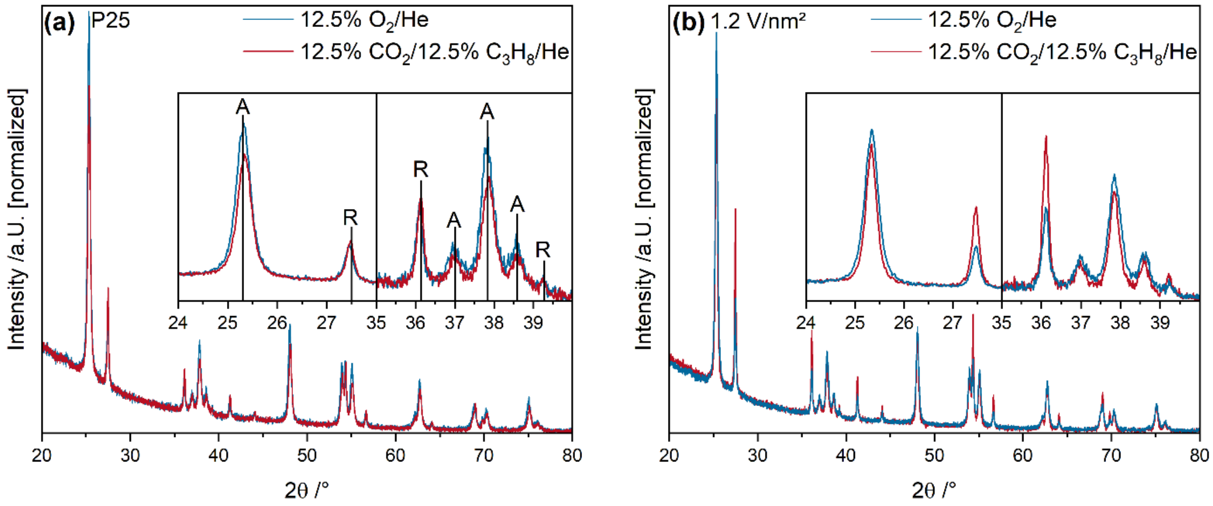

Figure 5: Quasi in-situ XRD patterns for **(a)** P25 and vanadia-loaded P25 with a loading density of **(b)** 1.2 V/nm² between 20 and 80° 2θ recorded after treatment in 12.5% O_2/He and the gas sequence up to 12.5% CO_2/12.5% C_3H_8/He at 550 °C, followed by rapid cooling to room temperature in He. The diffraction patterns were normalized and the inset shows selected regions in an enlarged view to highlight the relative intensity changes, where the detected reflexes are assigned to the anatase and rutile phases of TiO_2.

Figure 5a shows the quasi in situ XRD patterns of bare P25 recorded after pre-treatments in 12.5% O_2/He, and the gas sequence up to 12.5% CO_2/12.5% C_3H_8/He at 550 °C, followed by rapid cooling and inert transfer into the XRD sample holder. It can be seen that the amount of rutile in bare P25 stays unchanged, while the amount of anatase significantly decreases, which is in agreement with the Raman spectra and which indicates that bare titania reduces down to the bulk to regenerate the surface for the reaction.[57] This continuously reduces the titania to a point where the reaction slows down due to a depletion of available surface oxygen sites, which is reflected in the decreasing propane conversion (see Figure 2).

In comparison, Figure 5b shows the quasi in situ XRD patterns of the 1.2 V/nm² sample after the same pre-treatments as for bare P25. It shows a small decrease in the anatase intensity, while the rutile intensity simultaneously increases. This indicates that anatase is not reduced as in case of bare titania, but instead a phase transition towards a higher rutile content occurs. This was not observed during Raman spectroscopy, due to the small rutile intensity. This phase transition to rutile likely occurs since rutile activates CO_2 more easily than the anatase phase, as shown previously, to omit the bulk reduction and facilitate catalyst reoxidation.[58,59] This is catalyzed by the presence of vanadia, which can also be encapsulated in the titania during that transformation when it is present as V^{4+}, which is likely during the strongly reducing reaction conditions at 550 °C.[49] The fact that P25 does not show an increase in rutile during reaction might be caused by the lack of surface vanadia species catalysing this transformation. The transformation in the presence of V^{4+} species also correlates well with the increased conversions and the less pronounced reduction of titania, as rutile might regenerate the catalyst more quickly due to its easier CO_2 activation in addition to the surface vanadia species which might be able to participate in the redox cycle, increasing the overall amount of surface oxygen sites present for the reaction. On the other hand, the increased presence of rutile might also be responsible for the higher contribution of PDR occurring at higher loadings, which will be discussed in more detail in the DRIFTS section.

To obtain an integral picture of the reduction of all samples, including the reduction of vanadia, operando UV-Vis spectra were recorded and the structural changes observed were quantified. To gain insight into the temporal evolution of the catalysts, three spectra were recorded during the reaction and during the last regenerative phase. The results for P25 and the 1.2 V/nm² sample are depicted in Figure 6, whereas the UV-Vis spectra of the remaining samples are given in Figure S10 and those of the ALD-based samples are given in Figure S11.

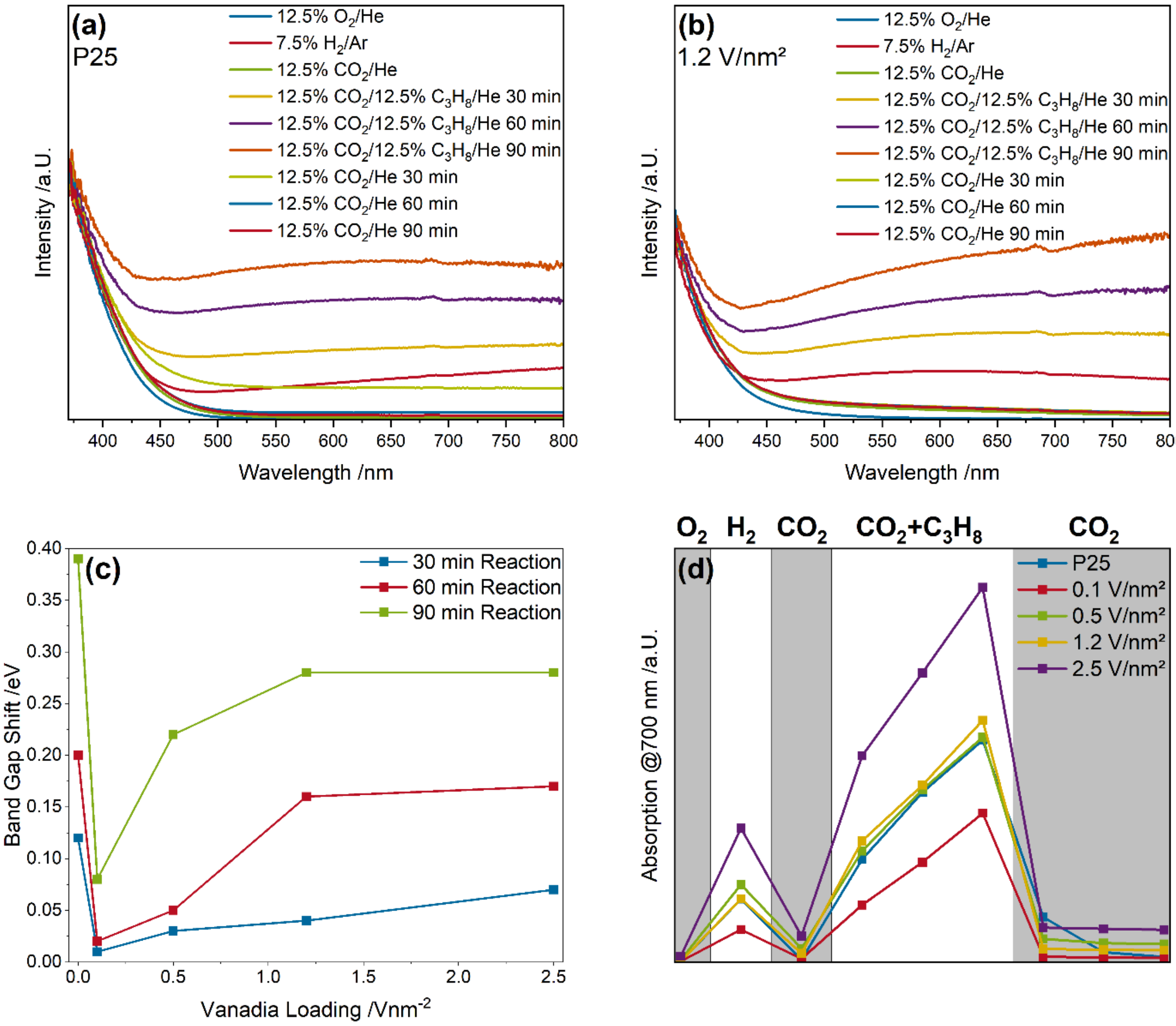

Figure 6: Operando UV-Vis spectra between 375 and 800 nm for **(a)** P25 and vanadia-loaded P25 with a loading density of **(b)** 1.2 V/nm² recorded at 550 °C in different gas feeds (see experimental section). Based on the UV-Vis spectra, the band gap energy shift **(c)** and the absorption at 700 nm (indicative of the degree of reduction) **(d)** were quantified. The spectra of the other P25-based samples are given in the SI (see Figure S10).

Figure 6a shows the operando UV-Vis spectra of bare P25. Two spectral changes can be observed, a shift in the band gap energy and an increase in the absorption between 500 and 800 nm. The red-shift in the band gap energy is associated with the reduction of titania and the subsequent creation of states within the band gap, lowering its energy,[60] while the increase in absorption between 500 and 800 nm originates from charge transfer between reduced and oxidized states of titania (Ti^{3+} to Ti^{4+}).[61,62] The observed red-shift in the band gap and the absorption increase between 500-800 nm correlate well with the reducibility of the corresponding gas phase. In comparison, the 1.2 V/nm² sample, shows the same kind of spectral changes, but with the vanadia causing an additional contribution in the region between 500 and 800 nm, due to the possibility of vanadia d-d transitions.[63]

Figures 6c and 6d summarize the results of the quantifications of the band gap shifts and the absorption increase between 500 and 800 nm for all samples. Starting with the band gap energies for the P25 sample a continuous red-shift of the band gap energy between 30 and 90 minutes is observed, with a shift of 0.4 eV in total, indicating a strong reduction of titania that cannot be explained by a phase transition that increases the amount of rutile, as bare P25 only reduces the anatase phase (see Figure 5). In comparison, the samples loaded with 0.1 and 0.5 V/nm² show almost no red-shift during the first 60 minutes, which however significantly increases after 90 minutes, indicating the much slower reduction of titania, in good agreement with the results from UV- and Vis-Raman spectroscopy. The phase transition from anatase to rutile, catalyzed by V^{4+}, might red-shift the band gap energy, as rutile has a lower band gap energy than anatase.[64,65] This seems to be especially true for the 0.5, 1.2, and 2.5 V/nm² samples, showing a significant shift in their band gap energy, despite their lack of subsurface reduction, which is likely caused by the larger transformation of anatase to rutile, as more vanadia is present on the catalyst to catqalyze the transformation.

The above findings are confirmed by the quantification of the absorption between 500 and 800 nm (see Figure 6d). During reaction conditions, P25 shows a continuously increasing absorption indicative of titania reduction due to $Ti^{3+} \rightarrow Ti^{4+}$ transitions, in agreement with the band gap energy shift and previous results. The introduction of small amounts of vanadium (0.1 V/nm²) leads to a smaller increase in absorption, that indicates significantly less titania reduction, particularly when considering the contribution of vanadia d-d transitions. This behavior is in agreement with the band gap energy shift and shows that this sample is not as strongly reduced as bare titania, as a result of increased regeneration via CO_2. At higher loadings (0.5 and 1.2 V/nm²) the absorption behavior resembles that of bare P25, likely caused by the increased amount of vanadia participating in d-d transitions. The latter contribution further increases for the 2.5 V/nm² sample. Overall, the intensity of d-d transitions correlates well with the observed conversions, indicating the participation of vanadia in the reaction mechanism.

To obtain a more detailed understanding of surface adsorbates and the contribution of different vanadia species, quasi in situ DRIFTS was performed, following the procedure as in case of the XRD measurements (see Figure 5). Figure

7a depicts the DRIFT spectra of P25+1.2 V/nm², while Figure 7b shows the difference spectra for all five samples. Figures 7c and d summarize the quantification results of the V=O and Ti-OH regions, respectively. The DRIFT spectra of the remaining P25-based samples and the ALD-based samples are given in the Si (see Figures S12 and S13).

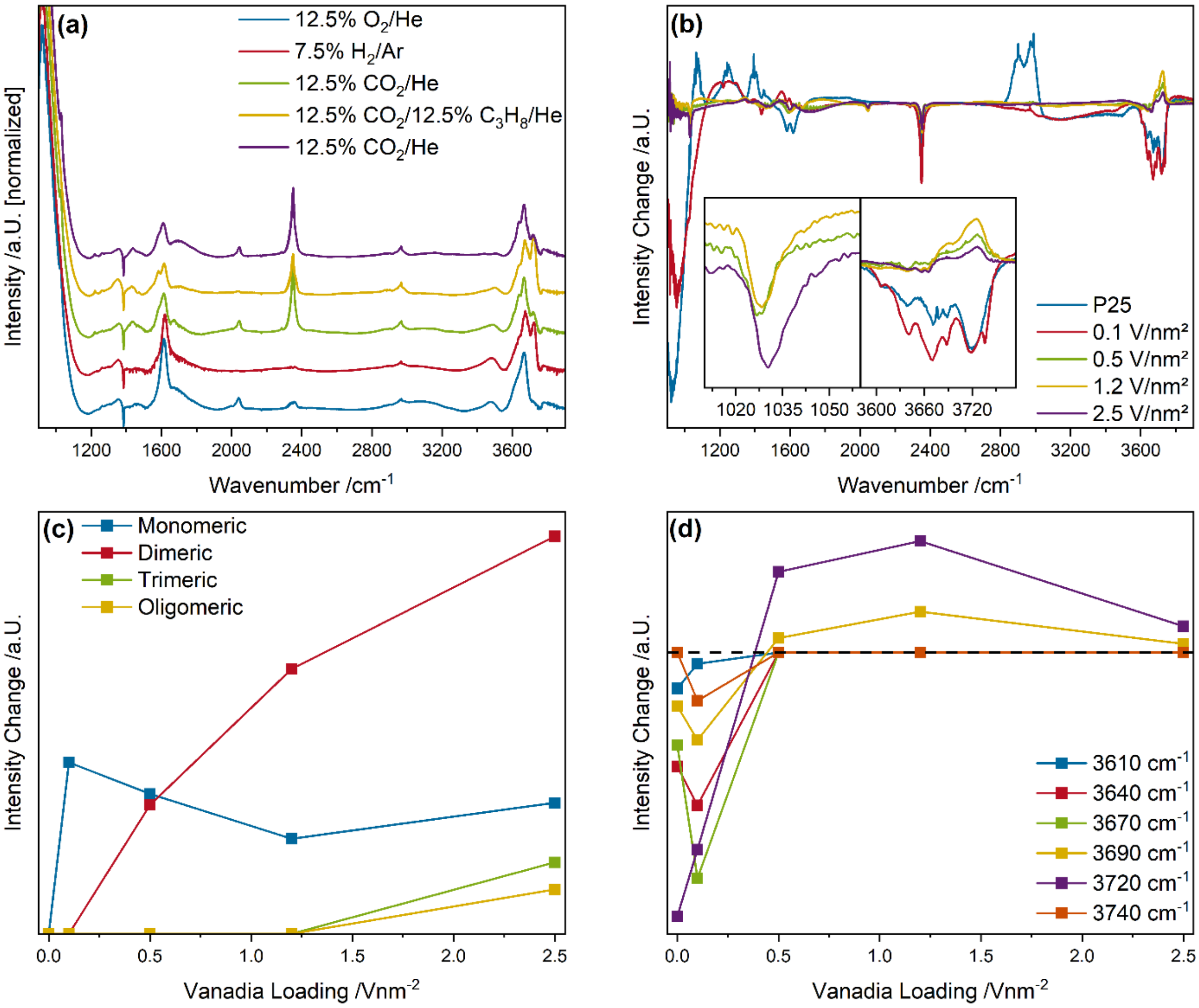

Figure 7: (a) Quasi in-situ DRIFT spectra of the 1.2 V/nm² sample recorded after treatment in different gas feeds (see experimental section) at 550 °C and subsequent rapid cooling to room temperature in He. The spectra were normalized and offset for clarity. **(b)** Difference between the spectra recorded in 12.5% CO_2/12.5% C_3H_8/He and 12.5% CO_2/He for P25 and vanadia-loaded samples. The insets highlight the intensity changes in the V=O region (0.5, 1.2, and 2.5 V/nm²) and in the Ti-OH region (all samples). The horizontal dashed line indicates no change in intensity. Loading-dependent quantification of **(c)** the intensities of different nuclearities in the V=O region and **(d)** the different contributions to the Ti-OH region. The quasi in-situ DRIFT spectra of the other P25-based samples are given in the SI (see Figure S12).

As shown in Figure 7a, in the DRIFT spectra of the 1.2 V/nm² sample differences in the V=O and Ti-OH region can be recognized, that are clearly visible in the difference spectra between oxidative (12.5% O_2/He) and reactive (12.5% CO_2/12.5% C_3H_8/He) conditions (see Figure 7b). Here, in agreement with the previous spectroscopic data on the TiO_2 reducibility, the P25 and P25+0.1 V/nm² samples show a strong intensity decrease in the feature at ~925 cm^{-1}, originating from the Ti-O vibration of Ti-OH species, which indicates strong surface reduction compared to oxidative conditions. The samples with higher vanadia loadings do not show these differences, but rather a pronounced decrease in the vanadyl region (see left inset). In the carbonate region almost no changes are observed, indicative of the absence of surface adsorbates (based on DRIFTS), while different Ti-OH species participate in the reaction for all samples (see right inset). The intensity changes in the vanadyl and Ti-OH region are summarized in Figure 7c and d, respectively.

Starting with the vanadyl contributions in Figure 7c, the 0.1 V/nm² sample shows only one highly symmetric contribution that was previously attributed to a monomeric species.[28] For the samples loaded with 0.5 and 1.2 V/nm², an asymmetric vanadyl feature with an additional contribution at higher wavenumbers is observed, which was previously assigned to dimeric species.[28,66–68] For the P25+2.5 V/nm² sample, additional peaks at higher wavenumbers are observed that can be attributed to trimeric and oligomeric species, which is in agreement with the increased vanadia d-d absorption (see Figure 6).[28,66–68] The contribution of monomers drops with increasing vanadium loading in favor of a significantly increased contribution of dimers, while all species show an increased contribution for the highest loading. As the quantification is performed on the basis of difference spectra, it is assumed that all of these species are either reduced or participating in the reaction mechanism leading to the ODH or PDR reaction. The participation of monomeric vanadia can be observed both in the increase in CO_2 and propane conversion (see Figure 2). Furthermore, it reduces the deep reduction of titania (see Figure 6) compared to P25, while still being heavily reduced to the low amount of VO_x. In comparison, no deep reduction of titania is observed for the 0.5 V/nm² sample, higher vanadium loading. However, at even higher loadings, an increasing amount of dimeric and oligomeric species is present on the catalyst surface. For these loadings, the PDR rate increases again, which seems to indicate that dimeric and oligomeric species are more active in the PDR rate, even though the reduction of titania is even further reduced. For the 2.5 V/nm² sample, this is likely caused by the presence of highly reducible linear V-O-V bonds of oligomeric vanadia,[28,67,68] that may be prone to the PDR reaction but also further increase the amount of converted propane and CO_2 compared to the 1.2 V/nm² sample, despite the similar PDR rate. These highly reducible vanadia bonds might also be responsible for the initial jumps in the CO_2 and C_3H_8 conversions as well as the PDR rate (see Figure 2), which in the course of the reaction decrease towards a lower level, indicating that these bonds might not be regenerated after the initial reaction. In total, the sum of monomeric and dimeric species correlates well with the observed increase in conversion (see Figure 2), indicating their participation in propane conversion.

Figure 7d summarizes the loading-dependent quantification of the Ti-OH related intensity changes. Bare P25 and the P25+0.1 V/nm² sample show a strong decrease in the intensity of all Ti-OH signals present, as the surface of the catalyst is heavily reduced and most Ti-OH bonds are consumed during reactive conditions. This is emphasized by the DRIFT spectra for the reactive and last regenerative gas phase (see Figure S12). Therefore, the decrease in Ti-OH species for these samples is not related to the reaction mechanism, but rather to catalyst deactivation. In comparison, the samples with higher vanadium loadings show an increase in the intensity of Ti-OH species located at 3690 and 3720 cm^{-1}, which are assigned to bridged and isolated Ti-OH species, respectively.[69–72] Bridged Ti-OH species have previously been associated with hydrogen storage during ODH reaction, thus acting as observer species, while isolated Ti-OH species were reported to be actively involved in the hydrogen transfer from propane to the catalyst.[28] Notably, no intensity change at the position associated with V-OH species is detected, indicating either a very fast or no involvement in the reaction mechanism. The intensity changes of both Ti-OH correlate with the conversion for the 0.5 and 1.2 V/nm² samples. However, for the 2.5 V/nm² sample, only smaller changes are observed, which might be explained by the presence of different vanadia nuclearities, that is oligomers, changing the reaction mechanism and increasing the PDR rate.

Finally, to further elucidate the main route of deactivation for the catalysts, a long-term catalytic experiment during reaction conditions with different CO_2 concentrations was performed (see Figure 8). This was motivated by the fact that the samples with higher vanadium loadings, which are not being as heavily reduced as bare P25, still show a decrease in propane conversion while staying constant in their

CO_2 consumption, indicating that they might be reduced very slowly. For these experiments, the 0.5 V/nm² sample was chosen, as it shows less reduction than the lower loadings without the PDR influence of the higher loadings. The results are normalized to the initial propane conversion to emphasize the decrease observed over time (see Figure 8).

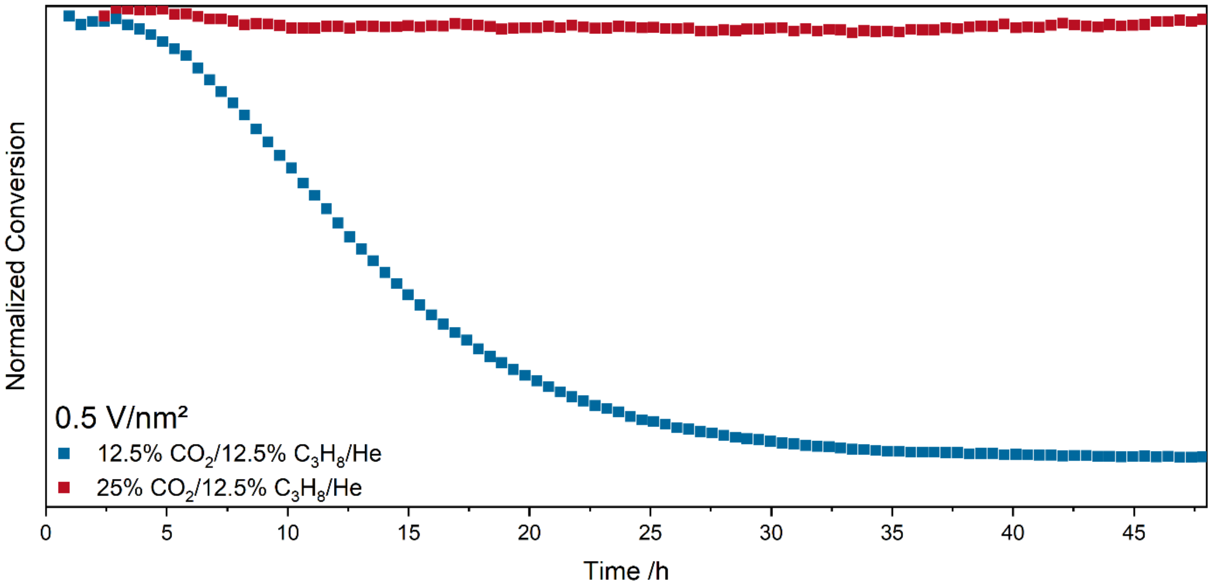

Figure 8: Long-term analysis of the propane conversion of the 0.5 V/nm² sample with CO_2/C_3H_8 gas-phase ratios of 1:1 (blue) and 2:1 (red) at 550 °C. The initial conversions were normalized for better comparability.

For a 1:1 ratio of CO_2/C_3H_8, the conversion ratio stays constant for the first 3 h before decreasing continuously to 10% of the initial conversion. In contrast, when increeasing the CO_2/C_3H_8 ratio to 2:1, the conversion stays constant over the full duration of the run (48 h). This behavior indicates that, first, catalyst deactivation also occurs for the higher loadings but at a lower rate, which is outside the range of our spectroscopic experiments, and second, that an increase in CO_2 conversion can stop the catalyst deactivation. Three main deactivation routes were observed in our spectroscopic experiments, that is, carbon deposition on the surface, deep reduction of the catalyst, and V^{4+} integration into titania. The first two might be impeded by the increased amount of CO_2 due to either an increased rate of regeneration or increased reaction of deposited carbon with CO_2 towards CO. The integration of vanadia into titania seems to be an important path, at least for the 1.2 and 2.5 V/nm² samples, since the decrease in propane conversion accelerates towards these loadings and might be caused by CO_2 being unable to reoxidize V^{4+} states, which can then only migrate into the titania lattice.[27] However, the conversion behavior might also be caused by the reduction of different vanadia speices as discussed above (see Figure 7). In addition, bare titania and the samples loaded with 0.1 and 0.5 V/nm² also show a decrease in propane conversion where the most likely deactivation mechanism occurs to be the deep reduction of the catalyst, since the ALD-based samples show no dynamics in the titania phonons or their band gap (see Figures S6, S9, and S11) and had a constant conversion during the catalytic test. However, these samples show significant amounts of carbon during reaction conditions (see Figure S6), which may indicate that carbon deposition is a less important deactivation mechanism. In addition, due to the different titania structure, titania does not seem to transform from anatase to rutile and to incorporate vanadia, as vanadyl dynamics can be observed for these samples (see Figure S6). Overall, the deactivation due to deep reduction seems to be the main deactivation route for the studied VO_x/TiO_2 catalysts, which can be impeded by an increase in the gas concentration of CO_2 leading to an increased rate of regeneration.

Mechanistic Discussion

The reaction mechanism of the CO_2-assisted propane ODH over VO_x/TiO_2 can be categorized according to the vanadium loading, that is, behavior at (near)zero loading (0 and 0.1 V/nm²), at medium loadings (0.5 and 1.2 V/nm²), and at high loading (2.5 V/nm²). As first step, hydrogen transfer is proposed to precede from propane to the titania surface for all samples (see Figure 7), followed byformation of water and an oxygen vacancy in the titania lattice. This is regenerated by oxygen diffusion from the subsurface/bulk for the bare P25 and 0.1 V/nm² samples, leading to a deep reduction of the catalyst, which especially favors the PDR reaction as already observed for the bare support of the VO_x/In_2O_3 system. No adsorbed intermediates are observed for any of the samples, indicating that the reaction occurs with a very high selectivity towards propylene. The deep reduction of titania seems to be the main deactivation mechanism due to a reduced rate of regeneration (see Figure 8). Since there is no selectivity difference between the samples expect for the observed PDR rate, only the identified structures responsible for the ODH rate are discussed.

The vanadia-loaded samples are proposed to undergo a similar hydrogen transfer but are heavily reduced themselves (see Figures 3, 6, and 7), indicating their participation in the reaction mechanism by delivering oxygen to drive the reaction. In addition, the rate of surface reoxidation by gas-phase activation of CO_2 is significantly increased due to the presence of vanadia, which is confirmed by the increased CO_2 conversion with increasing vanadium loading, despite the reduced PDR rate (see Figure 2). This is further supported by the conversion behavior, which increases linearly with the vanadium loading, emphasizing its importance for the conversion. The presence of vanadia may facilitate the CO_2 activation in two ways: First, the reduced vanadyl peak can activate CO_2 itself, regenerating the catalyst, and second, vanadia reduced to oxidation state V^{4+}, can catalyze the transformation of anatase into rutile (see Figure 5), which is much more active towards CO_2 and might thereby regenerate titania much faster. This is emphasized by the point that the titania reduction decreases with increasing vanadium loading. In fact, for the 2.5 V/nm² sample, even the surface of the catalyst is barely reduced. The integration of V^{4+} into the lattice is further supported by the fact, that for the samples with a notable formation of rutile during reaction conditions, no vanadia-related signals are observed (see Figure 3), while for the ALD-based samples, the structural dynamics of the vanadyl peak is clearly visible but no dynamics in the titania lattice due to the highly amorphous nature of the film, is observed.

Regarding the nuclearity dependence of the reactivity behavior, the increase in conversion correlates well with the sum of monomeric and dimeric vanadia species (see Figure 7), as previously observed for the reaction with O_2, indicating its importance as the oxygen site for the reaction. Therefore, a transfer of hydrogen from the titania lattice to vanadia is likely, followed by its integration into the lattice or a fast reduction to water due to the elevated temperatures. This is indicated by the clear reduction of vanadia (see Figures 6 and 7) while no V-OH species are present (see Figure 7d). The higher nuclearities, especially the linear V-O-V bonds of oligomeric vanadia species seem to favor the PDR significantly and react quickly at the beginning of the reaction (see Figures 2 and 7). The sample with 0.5 V/nm² shows almost no PDR, while showing a selectivity of close to 100% with a very small contribution from cracking. This sample contains no vanadia species with higher nuclearity and is not deeply reduced, with the ability to form rutile during the reaction. These properties seem to be most important for pushing the selectivity towards the ODH reaction.

4. Conclusion

In this study, we addressed the CO_2-assisted ODH of propane over VO_x/TiO_2 catalysts and elucidated important structural features relevant to the catalytic performance and the catalyst deactivation, by using multiple operando and quasi in situ methods. To unravel the role of the catalyst properties, we varied the vanadium loadings (0-2.5 V/nm²) and used two different types of titania support material, that is bulk P25 and ALD-prepared thin film titania on silica.

The catalytic performance of the catalysts depends strongly on the vanadium loading. Bare P25 shows a lower conversion, with a contribution of significant amounts of PDR. With increasing in vanadium loading, there is an increase in the conversion of propane and CO_2, but over time, the propane conversion decreases, while the CO_2 conversion stays constant. The PDR rate decreases to zero for the 0.1 and 0.5 V/nm² samples, but increases again for the samples loaded with 1.2 and 2.5 V/nm², while staying significantly lower than that of bare P25. Besides dehydrogenation and PDR, no significant side reactions were observed, except for some cracking, which is mostly caused by the reactor.

As a result of the mechanistic analysis, three main reaction paths were identified. Titania lattice oxygen is an important oxygen site for the reaction, which is heavily reduced in bare P25 during reaction conditions, leading to a deep reduction of titania. As a result, the catalyst gradually deactivates, leading to a significant increase in PDR as the main side reaction. The introduction of vanadia leads to a better activation of CO_2, enabling faster catalyst regeneration, which may occur via two routes. First, hydrogen can be transferred from the titania lattice to vanadia, where it forms water and reduces the vanadia species, leaving an oxygen vacancy. Since vanadium activates CO_2 better than titania, it can be regenerated more easily by gas phase CO_2, which impedes titania deep reduction and increases the overall reaction rate, while also decreasing the PDR route. Second, one hydrogen can be abstracted from titania to vanadia, reducing it to V^{4+}, which can then catalyze the anatase to rutile transformation, whereby the vanadium is integrated into the titania bulk. The higher activation rate of CO_2 over rutile compared to anatase enables the titania to be less reduced and to achieve a higher oxidation rate.

The nuclearity-dependence of the reaction shows that both monomeric and dimeric species increase the reaction rate and decrease the PDR route, while being actively reduced. However, higher nuclearities (e.g. oligomers in the sample loaded with 2.5 V/nm²) exhibit highly reducible oxygen atoms, that increase the contribution of the PDR route. Therefore, a selectivity maximum for the ODH route and therefore for propylene is achieved at a medium vanadium loading between 0.1 and 1.2 V/nm², where almost 100 % propylene selectivity is achieved.

The main deactivation route is the catalysts deep reduction, which depletes the active oxygen sites, leading to a continuous decrease in propane conversion, while the CO_2 conversion stays constant. Further deactivation mechanisms include the depletion of vanadia surface species, as they become integrated into the newly formed rutile phase as well as the formation of carbon. However, the ALD-based samples exhibit strong carbon deposition, while no strong titania lattice reduction is observed and the conversion stays constant, indicating carbon deposition to be of lower importance. The deactivation of the catalyst can be avoided by increasing the CO_2 gas phase concentration.

Our results highlight the potential of combining multiple operando and quasi in situ approaches to investigate the reaction mechanism of CO_2 activation during propane ODH, which is a highly relevant reaction with the potential of technical application. The VO_x/TiO_2 catalysts showed a highly promising performance that is more selective than that of most other oxide-based systems and comparable to CrO_x catalysts. For the first time, the reaction mechanism including the complex interplay between surface vanadia and multi-phase TiO_2 was elucidated. With this knowledge the catalyst performance can be improved. Our approach is readily transferable to other systems that are still missing from the literature, e.g. VO_x/CeO_2, to understand the important support contribution to the performance of vanadia-based catalysts in CO_2 activation.

Declaration of Competing Interest

The authors declare that they have no known competing financial interests or personal relationships that could have appeared to influence the work reported in this paper.

Supporting Information

The supporting information contains additional information about the reactivity behavior and additional results from operando spectroscopic analysis.

Acknowledgements

The authors acknowledge Till Wissel for performing nitrogen-adsorption experiments and BET analysis. This work was supported by the Deutsche Forschungsgemeinschaft (DFG, HE 4515/11-1).

References

(1) Amghizar, I.; Vandewalle, L. A.; van Geem, K. M.; Marin, G. B. New Trends in Olefin Production. *Engineering* **2017**, *3* (2), 171–178. DOI: 10.1016/j.eng.2017.02.006.

(2) Cavani, F.; Ballarini, N.; Cericola, A. Oxidative dehydrogenation of ethane and propane: How far from commercial implementation? *Catal. Today* **2007**, *127* (1-4), 113–131. DOI: 10.1016/j.cattod.2007.05.009.

(3) Lavrenov, A. V.; Saifulina, L. F.; Buluchevskii, E. A.; Bogdanets, E. N. Propylene production technology: Today and tomorrow. *Catal. Ind.* **2015**, *7* (3), 175–187. DOI: 10.1134/S2070050415030083.

(4) Phung, T. K.; Le Pham, T. M.; Vu, K. B.; Busca, G. (Bio)Propylene production processes: A critical review. *J. Environ. Chem. Eng.* **2021**, *9* (4), 105673. DOI: 10.1016/j.jece.2021.105673.

(5) Carrero, C. A.; Schloegl, R.; Wachs, I. E.; Schomaecker, R. Critical Literature Review of the Kinetics for the Oxidative Dehydrogenation of Propane over Well-Defined Supported Vanadium Oxide Catalysts. *ACS Catal.* **2014**, *4* (10), 3357–3380. DOI: 10.1021/cs5003417.

(6) Carter, J. H.; Bere, T.; Pitchers, J. R.; Hewes, D. G.; Vandegehuchte, B. D.; Kiely, C. J.; Taylor, S. H.; Hutchings, G. J. Direct and oxidative dehydrogenation of propane: from catalyst design to industrial application. *Green Chem.* **2021**, *23* (24), 9747–9799. DOI: 10.1039/D1GC03700E.

(7) Baek, J.; Yun, H. J.; Yun, D.; Choi, Y.; Yi, J. Preparation of Highly Dispersed Chromium Oxide Catalysts Supported on Mesoporous Silica for the Oxidative Dehydrogenation of Propane Using CO_2 : Insight into the Nature of Catalytically Active Chromium Sites. *ACS Catal.* **2012**, *2* (9), 1893–1903. DOI: 10.1021/cs300198u.

(8) Kätelhön, A.; Meys, R.; Deutz, S.; Suh, S.; Bardow, A. Climate change mitigation potential of carbon capture and utilization in the chemical industry. *Proc. Natl. Acad. Sci. USA* **2019**, *116* (23), 11187–11194. DOI: 10.1073/pnas.1821029116. Published Online: May. 13, 2019.

(9) Baena-Moreno, F. M.; Rodríguez-Galán, M.; Vega, F.; Alonso-Fariñas, B.; Vilches Arenas, L. F.; Navarrete, B. Carbon capture and utilization technologies: a literature

review and recent advances. *Energ. Source A: Recovery, Util. Environ. Effects* **2019**, *41* (12), 1403–1433. DOI: 10.1080/15567036.2018.1548518.

(10) Al-Mamoori, A.; Krishnamurthy, A.; Rownaghi, A. A.; Rezaei, F. Carbon Capture and Utilization Update. *Energy Technol.* **2017**, *5* (6), 834–849. DOI: 10.1002/ente.201600747.

(11) Álvarez, A.; Borges, M.; Corral-Pérez, J. J.; Olcina, J. G.; Hu, L.; Cornu, D.; Huang, R.; Stoian, D.; Urakawa, A. CO2 Activation over Catalytic Surfaces. *Chem. Phys. Chem.* **2017**, *18* (22), 3135–3141. DOI: 10.1002/cphc.201700782. Published Online: Oct. 5, 2017.

(12) Jacquemin, M.; Beuls, A.; Ruiz, P. Catalytic production of methane from CO_2 and H_2 at low temperature: Insight on the reaction mechanism. *Catal. Today* **2010**, *157* (1-4), 462–466. DOI: 10.1016/j.cattod.2010.06.016.

(13) Lei, T.-q.; Cheng, Y.-h.; Miao, C.-x.; Hua, W.-m.; Yue, Y.-h.; Gao, Z. Silica-doped TiO_2 as support of gallium oxide for dehydrogenation of ethane with CO_2. *Fuel Process. Technol.* **2018**, *177*, 246–254. DOI: 10.1016/j.fuproc.2018.04.037.

(14) Atanga, M. A.; Rezaei, F.; Jawad, A.; Fitch, M.; Rownaghi, A. A. Oxidative dehydrogenation of propane to propylene with carbon dioxide. *Appl. Catal. B: Environ.* **2018**, *220*, 429–445. DOI: 10.1016/j.apcatb.2017.08.052.

(15) Gambo, Y.; Adamu, S.; Tanimu, G.; Abdullahi, I. M.; Lucky, R. A.; Ba-Shammakh, M. S.; Hossain, M. M. CO_2-mediated oxidative dehydrogenation of light alkanes to olefins: Advances and perspectives in catalyst design and process improvement. *Appl. Catal. A: Gen.* **2021**, *623*, 118273. DOI: 10.1016/j.apcata.2021.118273.

(16) Jiang, X.; Sharma, L.; Fung, V.; Park, S. J.; Jones, C. W.; Sumpter, B. G.; Baltrusaitis, J.; Wu, Z. Oxidative Dehydrogenation of Propane to Propylene with Soft Oxidants via Heterogeneous Catalysis. *ACS Catal.* **2021**, *11* (4), 2182–2234. DOI: 10.1021/acscatal.0c03999.

(17) Rigamonti, M. G.; Shah, M.; Gambu, T. G.; Saeys, M.; Dusselier, M. Reshaping the Role of CO_2 in Propane Dehydrogenation: From Waste Gas to Platform Chemical. *ACS Catal.* **2022**, *12* (15), 9339–9358. DOI: 10.1021/acscatal.2c01374.

(18) Botavina, M. A.; Martra, G.; Agafonov, Y.A.; Gaidai, N. A.; Nekrasov, N. V.; Trushin, D. V.; Coluccia, S.; Lapidus, A. L. Oxidative dehydrogenation of C3–C4

paraffins in the presence of CO_2 over CrO_x/SiO_2 catalysts. *Appl. Catal. A: Gen.* **2008**, *347* (2), 126–132. DOI: 10.1016/j.apcata.2008.05.037.

(19) Gashoul Daresibi, F.; Khodadadi, A. A.; Mortazavi, Y.; Huotari, S.; Ritala, M. Highly dispersed atomic layer deposited CrO_x on SiO_2 catalyst with enhanced yield of propylene for CO_2–mediated oxidative dehydrogenation of propane. *Mol. Catal.* **2022**, *526* (80–), 112396. DOI: 10.1016/j.mcat.2022.112396.

(20) Michorczyk, P.; Pietrzyk, P.; Ogonowski, J. Preparation and characterization of SBA-1–supported chromium oxide catalysts for CO_2 assisted dehydrogenation of propane. *Microporous Mesoporous Mater.* **2012**, *161*, 56–66. DOI: 10.1016/j.micromeso.2012.05.011.

(21) Wang, H.; Nguyen, T. D.; Tsilomelekis, G. Propane oxidative dehydrogenation using CO_2 over CrO_x/Fe–CeO_2 catalysts. *Catal. Sci. Technol.* **2023**, *13* (8), 2360–2369. DOI: 10.1039/D2CY01563C.

(22) Wang, Z.-Y.; He, Z.-H.; Li, L.-Y.; Yang, S.-Y.; He, M.-X.; Sun, Y.-C.; Wang, K.; Chen, J.-G.; Liu, Z.-T. Research progress of CO_2 oxidative dehydrogenation of propane to propylene over Cr-free metal catalysts. *Rare Met.* **2022**, *41* (7), 2129–2152. DOI: 10.1007/s12598-021-01959-y. Published Online: Mar. 11, 2022.

(23) Ascoop, I.; Galvita, V. V.; Alexopoulos, K.; Reyniers, M.-F.; van der Voort, P.; Bliznuk, V.; Marin, G. B. The role of CO_2 in the dehydrogenation of propane over WO_x–VO_x/SiO_2. *J. Catal.* **2016**, *335*, 1–10. DOI: 10.1016/j.jcat.2015.12.015.

(24) Balogun, M. L.; Adamu, S.; Ba-Shammakh, M. S.; Hossain, M. M. Promotional effects of CO_2 on the oxidative dehydrogenation of propane over mesoporous $VO_x/\gamma Al_2O_3$ catalysts. *J. Ind. Eng. Chem.* **2021**, *96* (20), 82–97. DOI: 10.1016/j.jiec.2020.12.022.

(25) Jiang, X.; Lis, B. M.; Purdy, S. C.; Paladugu, S.; Fung, V.; Quan, W.; Bao, Z.; Yang, W.; He, Y.; Sumpter, B. G.; Page, K.; Wachs, I. E.; Wu, Z. CO_2-Assisted Oxidative Dehydrogenation of Propane over VO_x/In_2O_3 Catalysts: Interplay between Redox Property and Acid–Base Interactions. *ACS Catal.* **2022**, *12* (18), 11239–11252. DOI: 10.1021/acscatal.2c02099.

(26) Jiang, X.; Lis, B. M.; Wu, Y.; Wachs, I. E.; Wu, Z. Effect of the Molecular Structure of Surface Vanadia on Activity and Regenerability of VO_x/In_2O_3 Catalysts for CO_2-

Assisted Oxidative Dehydrogenation of Propane. *J. Phys. Chem. C* **2023**, *127* (13), 6311–6320. DOI: 10.1021/acs.jpcc.3c00183.

(27) Rogg, S.; Hess, C. CO_2 as a soft oxidant for propane oxidative dehydrogenation: A mechanistic study using operando UV Raman spectroscopy. *J. CO2 Utiliz.* **2021**, *50* (9), 101604. DOI: 10.1016/j.jcou.2021.101604.

(28) Schumacher, L.; Pfeiffer, J.; Shen, J.; Gutmann, T.; Breitzke, H.; Buntkowsky, G.; Hofmann, K.; Hess, C. Collaborative Mechanistic Effects between Vanadia and Titania during the Oxidative Dehydrogenation of Propane Investigated by Operando and Transient Spectroscopies. *ACS Catal.* **2023**, 8139–8160. DOI: 10.1021/acscatal.3c01404.

(29) Balogun, M. L.; Adamu, S.; Bakare, I. A.; Ba-Shammakh, M. S.; Hossain, M. M. CO_2 Assisted Oxidative Dehydrogenation of Propane to Propylene over Fluidizable MoO_3/La_2O_3-γAl_2O_3 Catalysts. *J. CO2 Utiliz.* **2020**, *42*, 101329. DOI: 10.1016/j.jcou.2020.101329.

(30) Balogun, M. L.; Gambo, Y.; Adamu, S.; Ba-Shammakh, M. S.; Hossain, M. M. Kinetic modeling of oxidative dehydrogenation of propane with CO_2 over MoO_x/La_2O_3-Al_2O_3 in a fluidized bed. *AIChE J.* **2023**, *69* (3). DOI: 10.1002/aic.17903.

(31) Beck, B.; Harth, M.; Hamilton, N. G.; Carrero, C.; Uhlrich, J. J.; Trunschke, A.; Shaikhutdinov, S.; Schubert, H.; Freund, H.-J.; Schlögl, R.; Sauer, J.; Schomäcker, R. Partial oxidation of ethanol on vanadia catalysts on supporting oxides with different redox properties compared to propane. *J. Catal.* **2012**, *296*, 120–131. DOI: 10.1016/j.jcat.2012.09.008.

(32) Dinse, A.; Frank, B.; Hess, C.; Habel, D.; Schomäcker, R. Oxidative dehydrogenation of propane over low-loaded vanadia catalysts: Impact of the support material on kinetics and selectivity. *J. Mol. Catal. A: Chem.* **2008**, *289* (1-2), 28–37. DOI: 10.1016/j.molcata.2008.04.007.

(33) Jiang, X.; Manawan, M.; Feng, T.; Qian, R.; Zhao, T.; Zhou, G.; Kong, F.; Wang, Q.; Dai, S.; Pan, J. H. Anatase and rutile in evonik aeroxide P25: Heterojunctioned or individual nanoparticles? *Catal. Today* **2018**, *300*, 12–17. DOI: 10.1016/j.cattod.2017.06.010.

(34) Christodoulakis, A.; Machli, M.; Lemonidou, A. A.; Boghosian, S. Molecular structure and reactivity of vanadia-based catalysts for propane oxidative dehydrogenation studied by in situ Raman spectroscopy and catalytic activity measurements. *J. Catal.* **2004**, *222* (2), 293–306. DOI: 10.1016/j.jcat.2003.10.007.

(35) Spende, A.; Sobel, N.; Lukas, M.; Zierold, R.; Riedl, J. C.; Gura, L.; Schubert, I.; Moreno, J. M. M.; Nielsch, K.; Stühn, B.; Hess, C.; Trautmann, C.; Toimil-Molares, M. E. TiO_2, SiO_2, and Al_2O_3 coated nanopores and nanotubes produced by ALD in etched ion-track membranes for transport measurements. *Nanotechnol.* **2015**, *26* (33), 335301. DOI: 10.1088/0957-4484/26/33/335301. Published Online: Jul. 30, 2015.

(36) Waleska, P. S.; Hess, C. Oligomerization of Supported Vanadia: Structural Insight Using Surface-Science Models with Chemical Complexity. *J. Phys. Chem. C* **2016**, *120* (33), 18510–18519. DOI: 10.1021/acs.jpcc.6b01672.

(37) Antonov, L.; Nedeltcheva, D. Resolution of overlapping UV–Vis absorption bands and quantitative analysis. *Chem. Soc. Rev.* **2000**, *29* (3), 217–227. DOI: 10.1039/A900007K.

(38) Dolgonos, A.; Mason, T. O.; Poeppelmeier, K. R. Direct optical band gap measurement in polycrystalline semiconductors: A critical look at the Tauc method. *J. Solid State Chem.* **2016**, *240* (11), 43–48. DOI: 10.1016/j.jssc.2016.05.010.

(39) Filtschew, A.; Hofmann, K.; Hess, C. Ceria and Its Defect Structure: New Insights from a Combined Spectroscopic Approach. *J. Phys. Chem. C* **2016**, *120* (12), 6694–6703. DOI: 10.1021/acs.jpcc.6b00959.

(40) Bugrova, T. A.; Dutov, V. V.; Svetlichnyi, V. A.; Cortés Corberán, V.; Mamontov, G. V. Oxidative dehydrogenation of ethane with CO_2 over CrO_x catalysts supported on Al_2O_3, ZrO_2, CeO_2 and $Ce_xZr_{1-x}O_2$. *Catal. Today* **2019**, *333*, 71–80. DOI: 10.1016/j.cattod.2018.04.047.

(41) Buekens, A. G.; Froment, G. F. Thermal Cracking of Propane. Kinetics and Product Distributions. *Ind. Eng. Chem. Proc. Des. Dev.* **1968**, *7* (3), 435–447. DOI: 10.1021/i260027a022.

(42) Gomez, E.; Kattel, S.; Yan, B.; Yao, S.; Liu, P.; Chen, J. G. Combining CO_2 reduction with propane oxidative dehydrogenation over bimetallic catalysts. *Nat.*

Commun. **2018**, *9* (1), 1398. DOI: 10.1038/s41467-018-03793-w. Published Online: Apr. 11, 2018.

(43) Chen, L.; Allec, S. I.; Nguyen, M.-T.; Kovarik, L.; Hoffman, A. S.; Hong, J.; Meira, D.; Shi, H.; Bare, S. R.; Glezakou, V.-A.; Rousseau, R.; Szanyi, J. Dynamic Evolution of Palladium Single Atoms on Anatase Titania Support Determines the Reverse Water-Gas Shift Activity. *J. Am. Chem. Soc.* **2023**, *145* (19), 10847–10860. DOI: 10.1021/jacs.3c02326. Published Online: May. 5, 2023.

(44) Doherty, F.; Goldsmith, B. R. Rhodium Single-Atom Catalysts on Titania for Reverse Water Gas Shift Reaction Explored by First Principles Mechanistic Analysis and Compared to Nanoclusters. *ChemCatChem* **2021**, *13* (13), 3155–3164. DOI: 10.1002/cctc.202100292.

(45) Siahvashi, A.; Adesina, A. A. Hydrogen production via propane dry reforming: Carbon deposition and reaction-deactivation study. *Int. J. Hydrog. Energ.* **2018**, *43* (36), 17195–17204. DOI: 10.1016/j.ijhydene.2018.07.118.

(46) Balachandran, U.; Eror, N. G. Raman spectra of titanium dioxide. *J. Solid State Chem.* **1982**, *42* (3), 276–282. DOI: 10.1016/0022-4596(82)90006-8.

(47) Zhang, J.; Chen, X.; Shen, Y.; Li, Y.; Hu, Z.; Chu, J. Synthesis, surface morphology, and photoluminescence properties of anatase iron-doped titanium dioxide nano-crystalline films. *Phys. Chem. Chem. Phys.* **2011**, *13* (28), 13096–13105. DOI: 10.1039/c0cp02924f. Published Online: Jun. 21, 2011.

(48) Ishioka, K.; Petek, H. Raman generation of coherent phonons of anatase and rutile TiO_2 photoexcited at fundamental absorption edges. *Phys. Rev. B* **2012**, *86* (20). DOI: 10.1103/PhysRevB.86.205201.

(49) Martínez-Huerta, M. V.; Fierro, J.L.G.; Bañares, M. A. Monitoring the states of vanadium oxide during the transformation of TiO_2 anatase-to-rutile under reactive environments: H_2 reduction and oxidative dehydrogenation of ethane. *Catal. Commun.* **2009**, *11* (1), 15–19. DOI: 10.1016/j.catcom.2009.08.002.

(50) Glassford, K. M.; Chelikowsky, JR. Optical properties of titanium dioxide in the rutile structure. *Phys. Rev. B Condens. Matter* **1992**, *45* (7), 3874–3877. DOI: 10.1103/physrevb.45.3874.

(51) Daude, N.; Gout, C.; Jouanin, C. Electronic band structure of titanium dioxide. *Phys. Rev. B* **1977**, *15* (6), 3229–3235. DOI: 10.1103/PhysRevB.15.3229.

(52) Tang, H.; Berger, H.; Schmid, P. E.; Lévy, F. Optical properties of anatase (TiO_2). *Solid State Commun.* **1994**, *92* (3), 267–271. DOI: 10.1016/0038-1098(94)90889-3.

(53) Burcham, L. J. In situ IR, Raman, and UV-Vis DRS spectroscopy of supported vanadium oxide catalysts during methanol oxidation. *Top. Catal.* **2000**, *11/12* (1/4), 85–100. DOI: 10.1023/A:1027275225668.

(54) Kryukova, G. N.; Zenkovets, G. A.; Mestl, G.; Schlögl, R. Structural study of titanium doped vanadia and vanadium doped titania catalysts. *React. Kin. Catal. Lett.* **2003**, *80* (1), 161–169. DOI: 10.1023/A:1026000829726.

(55) Lejon, C.; Österlund, L. Influence of phonon confinement, surface stress, and zirconium doping on the Raman vibrational properties of anatase TiO_2 nanoparticles. *J. Raman Spectrosc.* **2011**, *42* (11), 2026–2035. DOI: 10.1002/jrs.2956.

(56) Hearne, G. R.; Zhao, J.; Dawe, A. M.; Pischedda, V.; Maaza, M.; Nieuwoudt, M. K.; Kibasomba, P.; Nemraoui, O.; Comins, J. D.; Witcomb, M. J. Effect of grain size on structural transitions in anatase TiO_2 : A Raman spectroscopy study at high pressure. *Phys. Rev. B* **2004**, *70* (13), 717. DOI: 10.1103/PhysRevB.70.134102.

(57) Tobaldi, D. M.; Pullar, R. C.; Seabra, M. P.; Labrincha, J. A. Fully quantitative X-ray characterisation of Evonik Aeroxide TiO_2 P25®. *Mater. Lett.* **2014**, *122*, 345–347. DOI: 10.1016/j.matlet.2014.02.055.

(58) Liu, L.; Zhao, H.; Andino, J. M.; Li, Y. Photocatalytic CO_2 Reduction with H_2O on TiO_2 Nanocrystals: Comparison of Anatase, Rutile, and Brookite Polymorphs and Exploration of Surface Chemistry. *ACS Catal.* **2012**, *2* (8), 1817–1828. DOI: 10.1021/cs300273q.

(59) Kovačič, Ž.; Likozar, B.; Huš, M. Electronic properties of rutile and anatase TiO_2 and their effect on CO_2 adsorption: A comparison of first principle approaches. *Fuel* **2022**, *328* (19), 125322. DOI: 10.1016/j.fuel.2022.125322.

(60) Amore Bonapasta, A.; Filippone, F.; Mattioli, G.; Alippi, P. Oxygen vacancies and OH species in rutile and anatase TiO_2 polymorphs. *Catal. Today* **2009**, *144* (1-2), 177–182. DOI: 10.1016/j.cattod.2009.01.047.

(61) Kuriechen, S. K.; Murugesan, S.; Paul Raj, S. Mineralization of Azo Dye Using Combined Photo-Fenton and Photocatalytic Processes under Visible Light. *J. Catal.* **2013**, *2013* (4), 1–6. DOI: 10.1155/2013/104019.

(62) Yang, J.; Bai, H.; Tan, X.; Lian, J. IR and XPS investigation of visible-light photocatalysis—Nitrogen–carbon-doped TiO_2 film. *Appl. Surf. Sci.* **2006**, *253* (4), 1988–1994. DOI: 10.1016/j.apsusc.2006.03.078.

(63) Lamoureux, B.; Singh, V. R.; Jovic, V.; Kuyyalil, J.; Su, T.-Y.; Smith, K. E. Structural and electronic properties of thermally evaporated V_2O_5 epitaxial thin films. *Thin Solid Films* **2016**, *615*, 409–414. DOI: 10.1016/j.tsf.2016.07.062.

(64) Choudhury, B.; Choudhury, A. Oxygen defect dependent variation of band gap, Urbach energy and luminescence property of anatase, anatase–rutile mixed phase and of rutile phases of TiO2 nanoparticles. *Phys. E* **2014**, *56*, 364–371. DOI: 10.1016/j.physe.2013.10.014.

(65) Landmann, M.; Rauls, E.; Schmidt, W. G. The electronic structure and optical response of rutile, anatase and brookite TiO_2. *J. Phys. Condens. Matter.* **2012**, *24* (19), 195503. DOI: 10.1088/0953-8984/24/19/195503. Published Online: Apr. 19, 2012.

(66) Lian, Z.; Deng, H.; Xin, S.; Shan, W.; Wang, Q.; Xu, J.; He, H. Significant promotion effect of the rutile phase on V_2O_5/TiO_2 catalysts for NH_3-SCR. *Chem. Commun.* **2021**, *57* (3), 355–358. DOI: 10.1039/d0cc05938b.

(67) Jaegers, N. R.; Lai, J.-K.; He, Y.; Walter, E.; Dixon, D. A.; Vasiliu, M.; Chen, Y.; Wang, C.; Hu, M. Y.; Mueller, K. T.; Wachs, I. E.; Wang, Y.; Hu, J. Z. Mechanism by which Tungsten Oxide Promotes the Activity of Supported V_2O_5/TiO_2 Catalysts for NO_x Abatement: Structural Effects Revealed by ^{51}V MAS NMR Spectroscopy. *Angew. Chem. Int. Ed.* **2019**, *58* (36), 12609–12616. DOI: 10.1002/anie.201904503. Published Online: Aug. 1, 2019.

(68) Hu, J. Z.; Xu, S.; Li, W.-Z.; Hu, M. Y.; Deng, X.; Dixon, D. A.; Vasiliu, M.; Craciun, R.; Wang, Y.; Bao, X.; Peden, C. H. F. Investigation of the Structure and Active Sites of TiO_2 Nanorod Supported VO_x Catalysts by High-Field and Fast-Spinning ^{51}V MAS NMR. *ACS Catal.* **2015**, *5* (7), 3945–3952. DOI: 10.1021/acscatal.5b00286.

(69) Primet, M.; Pichat, P.; Mathieu, M. V. Infrared study of the surface of titanium dioxides. I. Hydroxyl groups. *J. Phys. Chem.* **1971**, *75* (9), 1216–1220. DOI: 10.1021/j100679a007.

(70) Tanaka, K.; White, J. M. Characterization of species adsorbed on oxidized and reduced anatase. *J. Phys. Chem.* **1982**, *86* (24), 4708–4714. DOI: 10.1021/j100221a014.

(71) Hadjiivanov, K. I.; Klissurski, D. G. Surface chemistry of titania (anatase) and titania-supported catalysts. *Chem. Soc. Rev.* **1996**, *25* (1), 61. DOI: 10.1039/cs9962500061.

(72) Mathieu, M. V.; Primet, M.; Pichat, P. Infrared study of the surface of titanium dioxides. II. Acidic and basic properties. *J. Phys. Chem.* **1971**, *75* (9), 1221–1226. DOI: 10.1021/j100679a008.